VERIFICATION OF MULTIPLE MECHANISM MODEL FOR THE PHOTOLUMINESCENCE OF OXIDIZED POROUS SILICON AND NANOSILICON PARTICLE EMBEDDED IN SILICON OXIDE

A Thesis Submitted to the School of Graduate Studies of
Addis Ababa University

In Partial Fulfillment of the Requirements for the Degree Of
Masters of Science in
Physics

By

Wondwosen Tilahun Metaferia
(B.Sc, Addis Ababa University, 2004)

Advisor: Dr. Sib Krishna Ghoshal

Addis Ababa, Ethiopia

July, 2007

ADDIS ABABA UNIVERSITY

SCHOOL OF GRADUATE STUDIES

The undersigned hereby certify that they have read and recommended to the Faculty of Science School of Graduate Studies for acceptance a thesis entitled "**Verification of Multiple Mechanism Model for oxidized porous silicon and nanosilicon particle embedded in silicon oxide**" by **Wondwosen Tilahun** in partial fulfillment of the requirements for the degree of **Master of Science in Physics**.

Name	Signature
Dr. S. K. Ghoshal, Advisor	____________________
Prof. Singh P., Examiner	____________________
Dr. Tesgera Bedassa, Examiner	____________________

Addis Ababa, Ethiopia

July, 2007

© Copyright by Wondwosen Tilahun 2007
All Rights Reserved

ABSTRACT

The purpose of this thesis is to give a coherent explanation of the most debatable issue of highly efficient photoluminescence (PL) in the visible range found in oxidized porous Silicon (p-Si). In order to describe the PL mechanism, we considered three competitive processes, process (A) where in both photoexcitation and photoemission occur in the NSP, (B), in which photexcitation occurs in the NSP and photemission occurs in luminescence centers (LCs), in the Si-oxide layer surrounding the NSP, and (C) in which both photoexcitation and photoemission occur in the LCs. We used the first two processes to explain the optical process by the quantum confinement (QC) and quantum confinement luminescence center (QCLC) models. For the nanoscale Si/SiO_2 systems, the radiative recombination rates of processes A and B are compared qualitatively. Process that plays the major role in the PL is determined by the capture cross-section, the luminescence efficiency, and the density of the LCs and size of the NSPs, all of which are dependent on the oxidation degree of the p-Si sample. For a nanoscale Si/Si-oxide system with the LC having certain capture cross-section and luminescence efficiency, it is found that the higher the LC density and the larger the size of the NSPs, the more beneficial for the QCLCM process to surpass the QCM process and vise versa. For certain LC parameters, there is a critical most probable size of the NSPs. In case when the most probable size of the NSPs is larger than the critical one, the QCLCM process dominates the PL on the other hand if the most probable size of the NSPs is smaller than the critical one, the QCM process dominates the PL. Furthermore, if the most probable size is close to the critical one both processes should be taken in to account. In general, for a p-Si sample free from oxidation, the QCM process dominates and the model is important to describe the PL. For most oxidized p-Si, the QCLCM process dominates and the model is useful to describe the PL and when the NSPs in oxidized p-Si samples have very small density or very large size, the process that both photexcitation and photoemission occur in the LCs in the silicon-oxide layer dominating. Hence, the importance of more than one type of mechanism models to describe the PL from oxidized p-Si and NSP embedded in Si-oxide is verified.

Contents

List of Figures iii

1 Introduction **1**

1.1 Why Silicon? 1
1.2 Low Dimensional Silicon 4
1.2.1 Fabrication of Silicon Nanocrystal 8
1.3 Optical Properties of Low Dimensional Silicon 11
1.3.1 Light Emission from Si Nanocrystals and Quantum Confinement Effect 16
1.4 Si/SiO_2 Interfaces in $SiO_2/Si/SiO_2$ Multiple Quantum Wells 19
1.5 Thesis Organization 20

2 Photoexcitation-Photoemission Process in Si/Si-Oxide Systems **22**

2.1 Introduction 22
2.2 Light Emitting Silicon Nanocrystals in SiO_2 22
2.3 Optical Transitions in Si/SiO_2 Based Nanostructures 24
2.3.1 Quantum Confinement Effect on the Optical Transition in Si/SiO_2 Based Quantum Wells 28
2.3.2 Interface Mediated Transition 30
2.4 Photoluminescence Mechanism Models 32
2.4.1 Quantum Confinement Model 32
2.4.2 Surface State Model 35
2.4.3 The Quantum Confinment Luminescence Center Model 38

3 Mechanism Model for Recombination Rates in Si/Si-Oxide Systems **42**

3.1 Introduction 42
3.2 Radiative Recombination Rate for the QCM Process 44
3.3 Radiative Recombination Rate for the QCLCM Process 45

3.3.1 Limiting Cases 49
3.4 The Critical Luminescence Center Density 51
3.5 Radiative Recombination Rate for the LC Process 53

4 Results and Discussions 55
4.1 Photoluminescence Mechanism 55
4.2 Radiative Recombination Rate 57
4.3 Luminescence Center Density 59

5 Summary and Conclusion 65

6 Bibliograpy 68

List of Figures

1.1 Examples of Si nanophase structures: microporous (left), mesoporous (center) and macroporous (right). 4
1.2 The transition energy is calculated for the; lowest electron and heavy hole energies for infinite confining potential (Left) [4]. Band gap energy as a function of a diameter of crystalline Si spheres. The solid line is theorethical calculation by an effective mass approximation (right) [Kanemitsu et al]. 6
1.3 (a) Electronic energy gap as a function of the number of silicon atoms for different bond configurations. (b)Electronic energy gap as a function of the number of Si=O double bonds at the cluster [4]. 7
1.4 Silicon nanocrystal fabrication techniques. The three lower techniques produce Si-nc in a SiO_2 matrix. 9
1.5 Indirect (left) and Direct (right) transitions between valance band and conduction band. 12
1.6 Schematic diagram of Si nanocrystals in an amorpous matrix. Electron-hole pairs (dots) are locally excited. If the nanocrystal has a recombination center(star), the electron and hole recombine non-radiatively. If the nanocrystal is free of recombination centre, the electron and hole recombine radiatively [4]. 14
1.7 Schematic diagram of a Si-nc (left) and of the corresponding emission spectrum (right). The influence of the various processing parameters on the emission spectrum is shown by the arrows. 15
1.8 The resonant photoluminescence spectra of naturally (a) and heavily oxidized (b) p-Si. The arrows show the energy position of Si TA and TO momentum-conserving phonons with respect to the triple exciton ground state [9]. 16

2.1 Silicon nanocrystals embedded in SiO_2 23
2.2 Cross section of one SiO_2/Si/SiO_2 QW (left). Side view of Si/SiO_2 SLs model (with 5 bulk-like Si monolayers). The growth axis is the Si-(001) direction in both cases (right) [Lockwood et al]. 25

2.3 Schematic representation of light emmiting mechansim of $SiO_2/Si/SiO_2$ single quantum wells by (i) quantum confinment (PL_1) depending on Si thickness and (ii) Si-SiO_2 interface (PL_2). Reproduced from ref.[7]. . . 26
2.4 Schematic representation of quantum confinment by adjusting the Si layer thickness in $SiO_2/Si/SiO_2$ QWs. 29
2.5 First quantized energy level in $SiO_2/Si/SiO_2$ quantum well, assuming that SiO_2 has an infinite barrier [7]. 30
2.6 Room temperature PL from a Si/SiO_2 superlattice with d = 1.63 nm (right). The PL peak energy (open circles) and integrated intensity (full circles) at room temperature in Si/SiO_2 superlattices as a function of Si layer thickness. The solid line is the fit by effective mass theory [22]. 31
2.7 Schematic representation of one of the possible optical transitions leading to light emission in semiconductor, band-to-band recombination [20]. 33
2.8 Typical absorption and PL spectra of p-Si films (a) L= 2nm, (b) L =3.5nm, and (c) L= 9nm (left). Raman spectra of free standing p-Si films compared with the spectra calculated for a sphere of dimeter L (solid lines) (right) [22]. 35
2.9 Schematic of possible excitonic recombination paths (a) excitation: excited states (valence band) to excited states (conduction band); (b) dexcitation: conduction to valence band recombination; (c) relaxation: excited states to localized surface states (LSS) and (d) radiative recombination: LSS to ground states (left) [21]. Intrinsic surface state emission process (right) [20]. 36
2.10 Room temperature PL spectra from p-Si samples with different porosities kept under Ar atmosphere (a) and after exposure to air (b). . . . 37
2.11 Schematic illustration of electron-hole pairs recombining to emit visible light through luminescence centers, which are located in the SiO_2 layers,. a situation of case I [24]. 40

3.1 (a) Our schematic drawing of the QCLCM. The NSP and a LC are simplified as a cubic quantum box of side L and a small sphere. (b) The z-direction electron potential of a SiO_2 layer of thickness d adjacent to the NSP with side length L and of a LC located in the SiO_2 layer. . . . 46
3.2 Energy diagram of a LC. 47

4.1 The dependance of the radiative recombination rates on the size of the NSP for the two types of processes, QCM and QCLCM processes (from Eqn.(3.2) and (3.13)) 58
4.2 The critical luminescence density vs. the most probable size of the nanoscale silicon particle (from equation (3.22)) 60
4.3 PL spectra of Si nanoparticles (L=15-20) (left). PL spectra of Si nanoparticles (average size 5nm). As prepared and after aging [27]. 63
4.4 Schematic strength of the dominant factor in the PL [27]. 64

Acknowledgments

I feel a deep sense of gratitude to my advisor, Dr. Sib Krishna Goshal, for believing in me and the value of the thesis while patiently pursuing me to keep the schedule and meet deadlines in completing this thesis. He gave me invaluable guidance, advice and constructive comments.

Many friends with whom I had e-mail conversation have helped me a lot by providing recent journals for my work. More particularly I wish to thank the following four people: Addishiwot Girma, a diploma student at ICTP-Italy, Aysheshim Kebie, M.Sc student at the University of Alberta-Canada, Belay Zeleke, a PhD student at University of Rovira I Virgilli-Spain and Melaku Muluneh, a PhD student at the University of Harvard, USA.

My gratitude also goes to Addisu Gezahgn, Tizazu Habite and Tagel Assefa, who contributed significantly to this work.

Special thanks, respect and love must also goes to my fiance Eskedar Mulualem for her unreserved encouragement and assistance. She spent all of her time by thinking of me and the progress of my work.

Finally, I am indebted to my lecturers at the department of Physics, Addis Ababa University, for all what they did for me and my work one way or the other.

Chapter 1

Introduction

1.1 Why Silicon?

Bulk crystalline Silicon(c-Si) is the leading material in microelectronics and is one of the best studied of all materials. It is the workhorse in semiconductor device technology today. At present, Silicon-based device constitute the largest percent of all semiconductor devices sold world wide. Silicon dominance is the result of its band gap (i.e. 1.12 eV, ideal for room temperature operation and it is large enough to give relatively low leakage current from thermally generated carriers), its superb natural oxide, its outstanding mechanical properties and its abundance in nature. Silicon is unique in that it possesses the most outstanding natural dielectric, Silicon dioxide (SiO_2), which has high breakdown strength ($\approx$10 MV/cm) and low interface trap density ($\approx 10^9$ trap/cm^2). Silicon is an extremely hard, unyielding semiconductor with a knoop hardness of 1150 kg/mm^2 (twice that of stainless steel) and a yield strength of 7×10^{10}dyn/cm^2 (a factor of 1.8 larger than Tungsten). Silicon in the form of silica and silicates makes up 28% of the Earth's crust, and Silicon is second only to

oxygen in abundance. Si is yet the hardest (tiles in space shuttle) and softest (breast implantation).

Integration and economy of scale are the two key ingredients of the technological success of Si. The continuous improvements in Silicon technology have made it possible to grow and process 300mm wide single Si crystal at low cost and even larger crystals are now under development [1]. The high integration levels reached by the Silicon microelectronic industry in the nanometer range have permitted a whole electronic system to be included on a single chip (the System-on-Chip(SoC) approach). As this approach yields incredible processing capability and high speed device performance.

On the other hand, the bulk of Si wafer provides good mechanical support for the fabricated electronic devices, which reside in the region near the wafer's surface. A substitute material that has been suggested for some time was Gallium Arsenide (GaAs). However, the lack of native oxide, high processing cost and environmental concerns discourage the industry from the implementation of GaAs as an appropriate solution. The native oxide of Silicon (SiO_2) is used to fabricate Metal Oxide Semiconductor Field Effect Transistors (MOSFETs). These are the building blocks of that makes up Complimentary Metal Oxide Semiconductors (CMOS) circuits. With CMOS technology, it is possible to integrate millions of transistors on one chip. These are known as Ultra Large Scale Integrated (ULSI) circuits. Using Si based ULSI technology, the Semiconductor industry has greatly improved the efficiency to store, process and communicate information.

The idea of exploiting Silicon for light emitting device is appealing because it leads to the possibility of fabricating light emitting devices compatible with Si based optoelectronic integrated circuits. When this idea is realized device science will mark a revolutionary progress [2, 3].

The present semiconductor technology is to reduce the cost per function on a chip. Reducing the size of the device by reducing the size of each components in it without affecting the efficiency or with better efficiency (i.e. device scaling) is the method which takes much emphasis by the semiconductor industries all over the world. Therefore, the functionality of semiconductors at low dimension (1 and 2 dimensions) is realized in recent years. It is observed that the behavior of Silicon at nanometric scale become quite fascinating and peculiar.

To do this, Silicon nanotechnology has drawn considerable attention world wide for present day microelectronics technology. Nanotechnology may be identified as a technology where dimensions and tolerances in the range 0.1–100nm play a critical role. The active interest in this field is due to the significantly different properties of the materials compared with those of their bulk counterparts when they are synthesized and consolidated to create nanophase particles (figure 1.1). Nanometric structures represent an exciting, intellectually challenging, and rapidly expanding area of research that crosses the borders between many areas of the physical sciences and engineering. Since their properties can be engineered during the synthesis and processing steps by reducing the size of the crystals to nanosize range, cluster-assembled nanophase materials appear to have great technological potential.

Low dimensional Si is a fascinating material which has many unfold properties. Nanometer sized transistors are now switching in computers at working frequency exceedingly few GHz [4]. Subsequent research from the theoretical side has shown that, accompanying the reduction in sizes of a c-Si nanostructures, (*i*) the type of the band gap transforms from indirect to direct and (*ii*) the band gap-energy is blue shifted into the range of visible light owing to the quantum confinement effect [3]. Since the first observation of strong (room temperature) visible luminescence from nanosilicon it opened up new avenue for the possibility of using it for photonic device. We therefore, want to explain what is meant by nanosilicon and some of the optical properties of it.

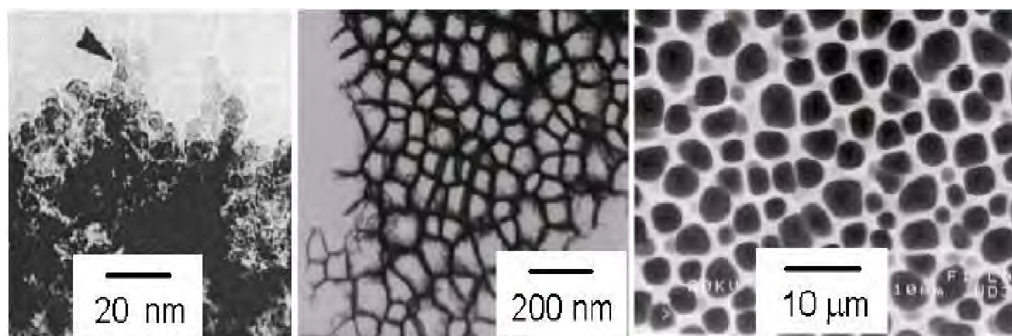

Figure 1.1: Examples of Si nanophase structures: microporous (left), mesoporous (center) and macroporous (right).

1.2 Low Dimensional Silicon

As we change the dimensionality of Si very fascinating and new optical properties of the material appear, light emission starts to be a very efficient process in nanostructured Si and light emitting diodes with efficiency in excess of 1% have been

fabricated [4]. Optical amplification has been also observed when Silicon nanocrystals are embedded into a dielectric matrix, such as SiO_2. This makes the Si in a dielectric matrix system a potential candidate for laser action. In addition to electronic property variations, nanostructured Si can also be used as nanodielectric material, where controlled changes in a refractive index can lead to trapping or slowdown of photons. In this and in the following sections we aim to give the explanation of low dimensional Si both it's electronic and it's dielectric properties.

The best way to understand the effects of the reduced dimensionality on the energy spectrum of an electron is to resort the particle in-a-box problem so familiar in quantum mechanics. With in the effective mass approximation in the envelope wave function description, the transition energy of an ectron-hole pair of effective reduced mass μ confined in a quantum dot[1] modeled as cubic box of sides L_x, L_y, and L_z is given by

$$E_{e,h} = E_g + \frac{\hbar^2}{2\mu}\left[\left(\frac{n_x\pi}{L_x}\right)^2 + \left(\frac{n_y\pi}{L_y}\right)^2 + \left(\frac{n_z\pi}{L_z}\right)^2\right], \tag{1.1}$$

where we have assumed that the confined energy barrier is of infinite strength and that E_g is the energy band gap of the bulk semiconductor, (i.e Silicon), n_x, n_y and n_z, are the quantum numbers to describe a given quantized energy level. Equation 1.1 shows that the effective energy band gap of the Silicon quantum dot increases as the quantum dot dimension decreases. If we assume the dot to be spherical, we have

$$E_{e,h} = E_g + \frac{\hbar^2}{2\mu}\left(\frac{n\pi}{d}\right)^2, \tag{1.2}$$

where d in the equation is the diameter of the dot. The transition energy scales with

[1]Quantum dot: It has all the 3-Ds in the nanorage. This means there is a total confinment in each direction and particles can't move freely anywhere. It is also known as a 0-D nanostructure.

a $\frac{1}{d^2}$ law. More accurate calculations show that the scaling law doesn't follow an exact power 2 law but instead the exponent is lower [4]. A value of 1.7-1.8 seems to be more appropriate. The transition energy and optical energy gap in quantum dot, quantum wires[2] and quantum wells[3] (Fig.1.2) increases as their size decreases.

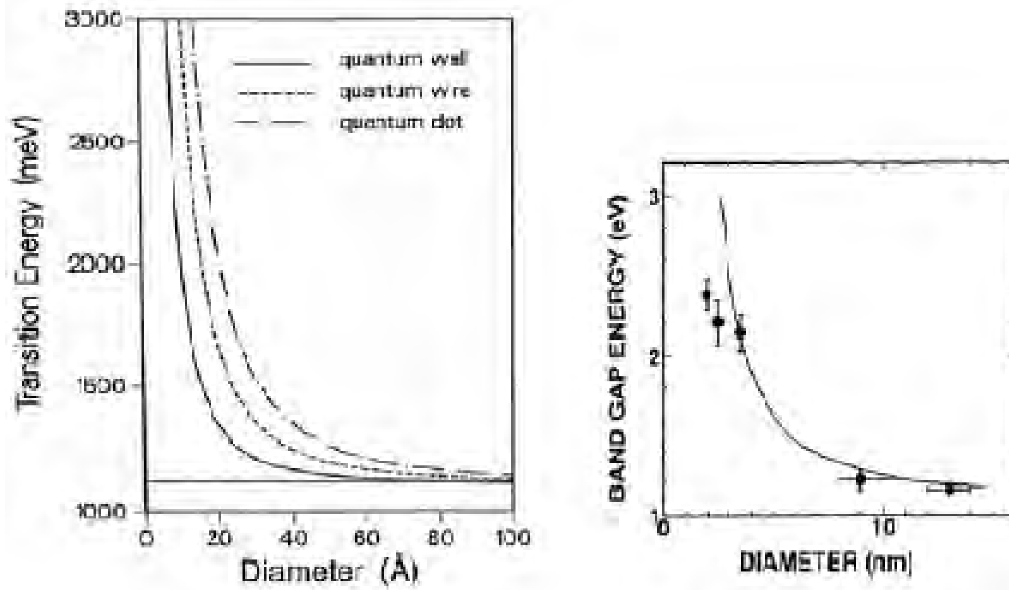

Figure 1.2: The transition energy is calculated for the; lowest electron and heavy hole energies for infinite confining potential (Left) [4]. Band gap energy as a function of a diameter of crystalline Si spheres. The solid line is theorethical calculation by an effective mass approximation (right) [Kanemitsu et al].

The assumption of having an infinite potential barrier is very crude since Silicon nanocrystals (Si-ncs) are usually formed in a dielectric matrix usually a silica glass (SiO_2) but more recently the use of Al_2O_3, Si_3N_4 or oxynitride is emerging as an alternative [4]. Also the effective mass approximation has strong limitation since the

[2]Quantum wire: It is a 1-D nanostructure where particles are free to move in only one direction. That is two sides of the structure are of nanometer length.

[3]Quantum well: it is a nanostructure where there are two directions for the movement of particles, while the third direction determines the quantum confinment direction. It is said to be a 2-D nanostructure.

reconstruction of the lattice in the dots caused by the strain and elastic properties of the host should be considered. Finally, chemical bonds among the surface Si atoms of the Si-nc and the atoms of the host, strongly modify the energy spectrum of Si-nc. Figure 1.3 shows the variation of the band gap as a function of bond configuration from a theoretical calculation.

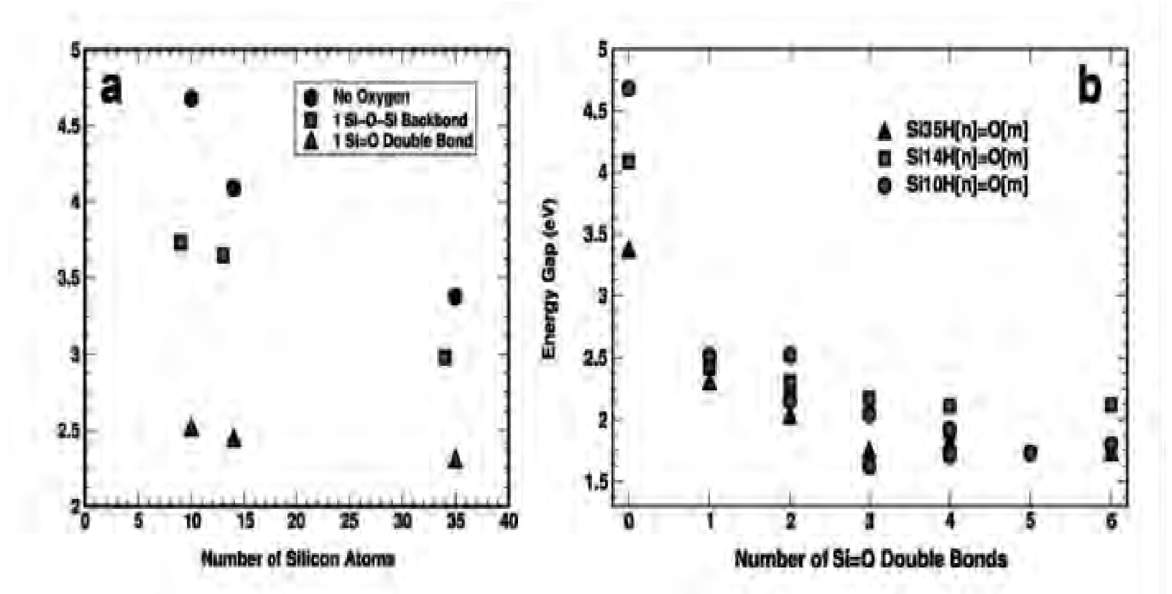

Figure 1.3: (a) Electronic energy gap as a function of the number of silicon atoms for different bond configurations. (b)Electronic energy gap as a function of the number of Si=O double bonds at the cluster [4].

In addition to the variation of the energy spectrum, also the wavefunctions of the electrons and of the hole are influenced by the reduced dimensionality in the dot. Overlap of the wavefunctions in real space and spreading of them in the **k**- space causes an increase in the optical transition probability by relaxing selection rules.

A quite indirect effect of the reduce dimensionality is the reduction of the effective refractive index of the composite matrix where the Si-ncs are formed. Indeed

in a simple scheme we can consider that the refractive index is an average of the refractive index of Si-nc and the host matrix. Thus, a composite layer formed by Si-nc with a large refractive index 3.5 dispersed in a matrix such as SiO_2 with refractive index of 1.45 [4] has a smaller refractive index than the bulk Silicon. The exact value depends on the Si content in the film and on the composition of the host dielectric. To see this, a simple approximation is usually used, the Bruggman approximation [1], in which it is assumed that a small particles of Silicon are dispersed in an host of dielectric function ε_m related to ε_{eff} as

$$f\frac{\varepsilon-\varepsilon_m}{\varepsilon+2\varepsilon_m}+(1-f)\frac{\varepsilon-\varepsilon_{eff}}{\varepsilon+2\varepsilon_{eff}}=0. \tag{1.3}$$

Here f is the volumetric fraction of Si and ε is the dielectric function. Using this formula refractive index $n=\sqrt{\varepsilon_{eff}}$ can be calculated. The reduction in the refractive index has a positive influence when the Si-ncs are used to enhance the emission efficiency of Si. Infact, the extraction efficiency of light from a material depends on its refractive index, the smaller n is the more the light is gathered. Much can be said about the optical properties of low dimensional Silicon, despite its various fabrication technique (figure 1.4). Now let us see how the fabrication of nanostructures are possible to realize device applications.

1.2.1 Fabrication of Silicon Nanocrystal

Since naked Silicon clusters are highly reactive they are mostly synthesized in a molecular beam under a high vacuum condition [5]. Present Silicon nanocrystals research is highly focusing on the preparation of Si-ncs embedded in an oxide

host. With regard to a strong photoluminescence (PL) of the nanocrystal Silicon in a visible range, the control of size, passivation and density is mandatory [5]. The size control is realized by changing the chemical stoichiometry of the sample. Reduction of the implanted Si dose or the oxygen enrichment is the usual way for the decreasing nanocrystal size. Silicon nanocrystals embedded in SiO_2 can be obtained by using several preparation techniques, such as laser ablation, aerosol technique, sputter decomposition, ion implantation, Chemical Vapor Deposition (CVD) or Plasma Enhanced Chemical Vapor Deposition (PECVD) [6]. However we can divid them into three main approaches: (a) Direct Synthesis of Si cluster, (b) Phase Separation, and (c) Electrochemical erosion of bulk Si.

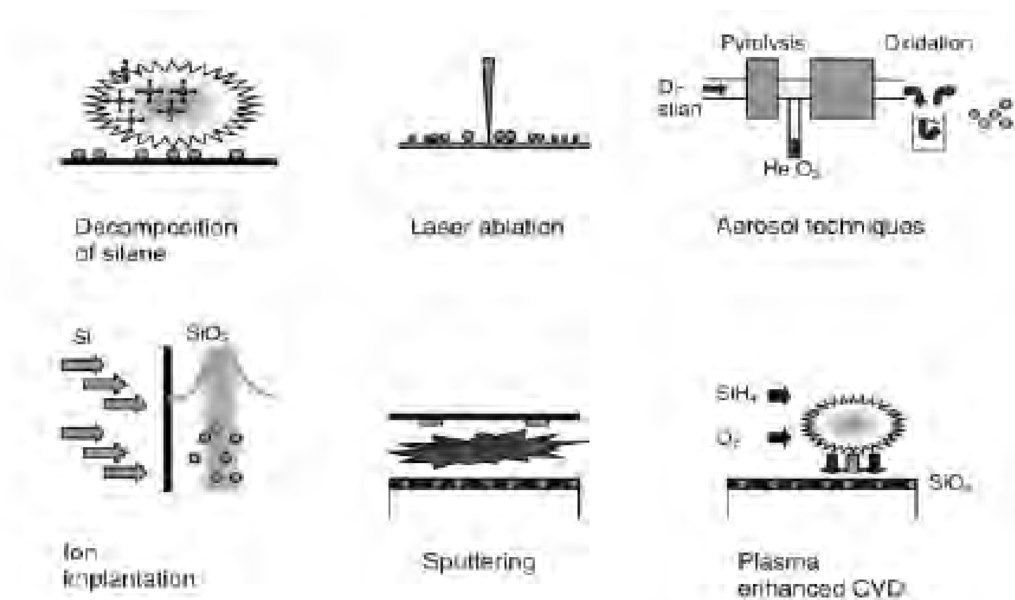

Figure 1.4: Silicon nanocrystal fabrication techniques. The three lower techniques produce Si-nc in a SiO_2 matrix.

1.2.1a Direct Synthesis of Silicon Clusters

Silicon nanoclusters can be directly synthesized by chemical reaction of suitable reactants. Method of synthesis of Si colloids include pyrolysis of Si_2H_6, formation by laser induced plasma in SiH_4, combustion of SiH_4, gas evaporation of Si and controlled neucletaion inside inverse micelles [2]. The end product is a colloidal suspension of Si-nc in solvent which is usually ethanol. Another way is to deposit Si-nc on a substrate after their formation in a molecular beam [5]. Within this approach one can also mass filter the cluster beam by time of flight method, which ends up with a size selection of the clusters.

1.2.1b Silicon Clusters Produced by Phase Separation

The formation of Si-nc by phase separation of Si rich dielectric is the most widely used approach. Various techniques have been employed to form the sub-stoichiometric dielectric, ion implantation, Plasma or Low-Pressure Chemical Vapor Deposition (PE-CVD or LP-CVD) [6], sputtering and Si evaporation. The differences among them are related to the degree of purity (better for ion implanted samples), to the degree of defects incorporated, to the porosity of the deposited film (which is known to be greater for the sputtered samples), to the control of the Si-nc content profile (better for the CVD films) [4]. After deposition the films are thermally treated at high temperature, to induce the phase separation between Si and the dielectrics. At the used temperatures Si difusivity is large enough to cause clustering but it is small enough to avoid significant bulk reconstruction.

1.2.1c Electrochemical Etching of Silicon

In this method of fabrication of low dimensional Si, porous Silicon (p-Si) is obtained by electrochemical etching of crystalline Si in Hydro Flueric acid (HF) rich electrolyte [4]. Following the partial wafer dissolution a porous structure is formed where the Si skeleton is composed either by interconnected Si-nc or by thin Si wires. What is astonishing in this process is the fact that the etching process is self regulated; once the porous layer is formed, no further etching of porous layer occurs. The reason for this is the depletion of holes in the etched region of the samples. Infact holes need to be exchanged with the electrolyte to achieve dissociation of Si. In addition, by suitable techniques, it is possible to form colloidal suspension for Si-nc by crumbling it into small particles. Si-nc solutions have been obtained by sonication of p-Si in acetonitrile and toluene, in acetone and other solvents. However it would be much more interesting to prepare Si-nc in water since most of its biological applications occur in aqueous environment. A simple sonication of naturally oxidized porous layer is shown to produce colloidal suspension in water [4].

1.3 Optical Properties of Low Dimensional Silicon

A semiconductor is characterized by a valence band that is filled or almost filled by electrons and an other energy band, conduction band which is empty and separated in energy by an amount E_g, the band gap energy, from the upper edge of the valence band. Photon absorption with electronic transitions from the valence band to states in the conduction band can takes place in these materials if the photon energy

$\hbar\omega \geq E_g$. Thus we can see that conduction in semiconductors requires a finite energy to promote the transition from the valence band to the conduction band. The energy

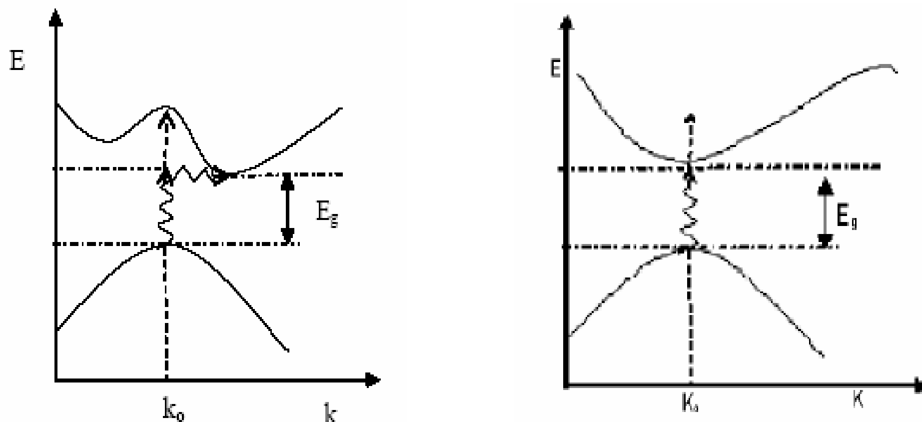

Figure 1.5: Indirect (left) and Direct (right) transitions between valance band and conduction band.

gap, the forbidden range of energies is of fundamental importance for the properties of solids in general. Most of the solid properties, such as intrinsic conductivity electronic or optical transitions depend on it (i.e. any change of the gap significantly alters the material's Physics and Chemistry). According to the band theory of solids, in solid state Physics bulk Si is an indirect band gap semiconductor, i.e the energy maxima in the valence band and minima in conduction bands do not occur at the same k-point. In an indirect band gap materials, the optical process should conserve the momentum of the electron in transition process, since the momentum of a photon is very small compared to the crystal momentum and transition is phonon mediated. On the other hand the conservation of momentum in a direct transition involves states having the same **k** values as shown in figure 1.5.

In addition, bulk crystalline Si is a centrosymmetric crystal that does not show efficient band to band light emission or PL. Several engineering solutions have been proposed to solve this limitation of Si. Some of these solutions include optically active impurity mediated luminescence with Er or iron-silicide ($FeSi_2$) and low dimensional Si structures (Si-nanostructures), Si-nanostructures with Brillouin zone folding including porous Si, superlattices and quantum wells [7]. In this section attention is given to the optical properties of low dimensional Si and the optical properties of Si-based multiple quantum wells will be treated latter in chapter 2.

In fact, the indirect band gap in bulk Si don't totally make light emission impossible but it causes a very long radiative life time (in the range of ms) for the excited electron-hole pairs. Competing non-radiative recombinations prevail and cause most of the excited electron-hole pair to recombine non-radiatively. In addition, when the number of excited electron-hole increases other non-radiative recombination process start to play a role. These are Auger recombinations and free carrier absorption. In Auger recombination process electron-hole pair recombines giving the excess energy to a third particle (an electron or a hole); free carrier absorption is a process for which the photon is absorbed by free carriers via an intra-band[4] optical transition.

Both the above mentioned processes are dependent on the density of excess free carriers and dominate the recombinations for heavily excited or doped Si. The hope in using nanocrystals was to increase the radiative recombination rate by exploiting quantum confinement effect. However, another effect also improved the emission efficiency of Si-nc and that is the spacial localization of excited electron-hole

[4]Transitions between subbands of different bands.

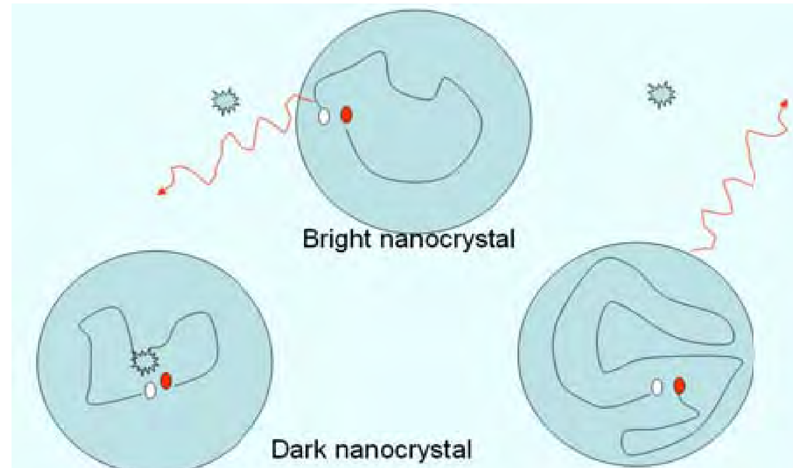

Figure 1.6: Schematic diagram of Si nanocrystals in an amorpous matrix. Electron-hole pairs (dots) are locally excited. If the nanocrystal has a recombination center(star), the electron and hole recombine non-radiatively. If the nanocrystal is free of recombination centre, the electron and hole recombine radiatively [4].

in a small region of the sample. If this region has a killer (recombination) centre, the nanocrystal is dark, on the contrary, if it is free of killer centers, the nanocrystal is bright and the excited electron-hole recombines radiatively, even though with a long life time as depicted in figure 1.6.

Room teperature emission in Si-nc is routinely observed independently on the preparation method. The emission is usually characterized by a first band centred at about 500nm whose position is independent of the processing parameters use to form the Si-nc and a second band in the wavelength range 600-900nm [4], whose exact spectral position depends strongly on the process parameters as indicated in figure 1.7. The first band is defect related and can be quenched by post-growth passivation with hydrogen [4]. It is absent in sample of high quality. The second is related to the presence of the Si-nc; when the size of Si-nc decreases due to a low Si content in

the deposited film or to allow annealing temperature treatments, the emission band shifts to the blue. On the contrary for high Si content in the film or high annealing temperature the emission band shows a red shift.

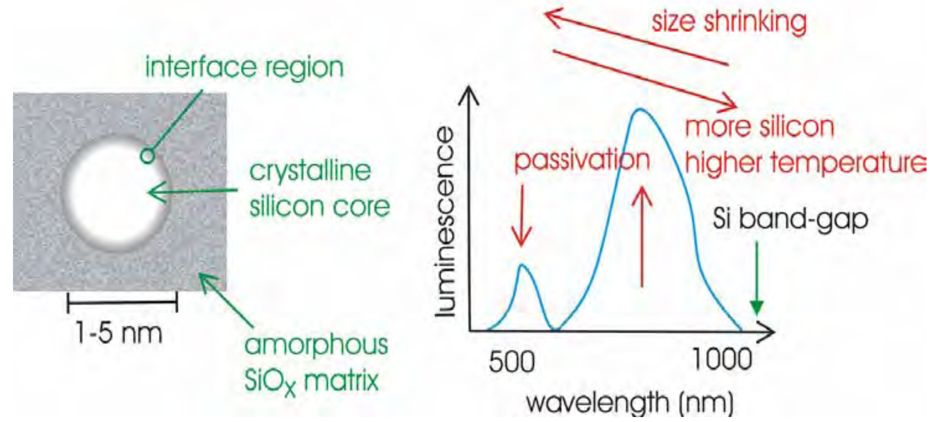

Figure 1.7: Schematic diagram of a Si-nc (left) and of the corresponding emission spectrum (right). The influence of the various processing parameters on the emission spectrum is shown by the arrows.

The exact origin of the emission is not clear. Certainly the reduced dimensionality effect in Si crystal plays a crucial role. However, as the photoluminescence characteristics are determined by both the quantum confinment and surface passivation, the role of the surface cannot be neglected [8]. As shown in figure 1.7, the structure of the Si-nc is formed by three regions: the central region made of amorpous or crystalline Si, the interface region made of substoichiometric and stressed silica and the embedding amorphous dielectric. Resonant PL experiments have shown that the emission spectrum which is interpreted in terms of crystalline Silicon phonon assisted recombination as shown in figure 1.8 [9]. These data are interpreted in the frame work of a pure quantum confinement process. Other experiments on the other hand, have

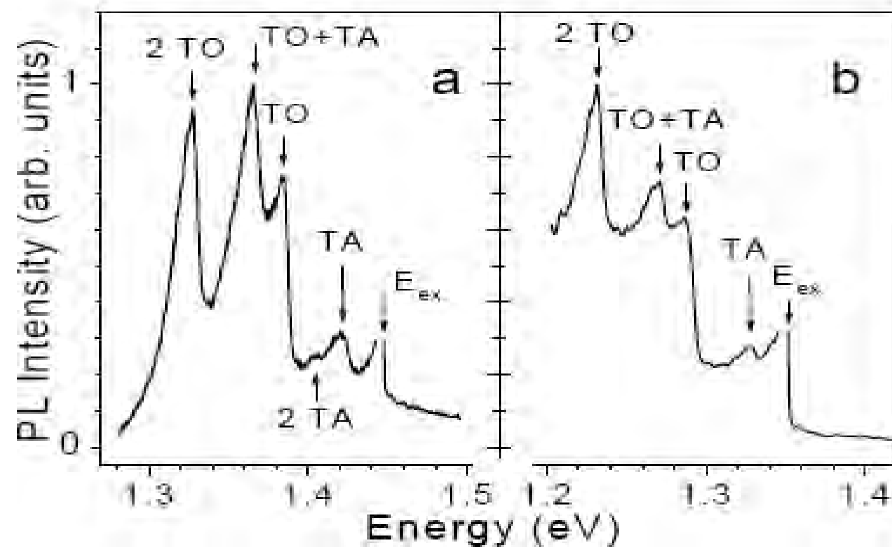

Figure 1.8: The resonant photoluminescence spectra of naturally (a) and heavily oxidized (b) p-Si. The arrows show the energy position of Si TA and TO momentum-conserving phonons with respect to the triple exciton ground state [9].

shown that the emission is strongly dependant on the exposure to ambient oxygen which seems to support a key role played by Si=O bond in the emission process [4].

1.3.1 Light Emission from Si Nanocrystals and Quantum Confinement Effect

Quantum confinement of electrons and holes within small nanocrystals incorporated into sensitive areas of a device might enhance the photonic capability of Silicon to such a degree that efficient Silicon-based light emitters may be realized. Light can be emitted when an electron recombines with a hole in the semiconductor. To make it efficient, the electron and the hole must be close enough to each other to have overlapping momentum distributions and hence the wavefunction. Unfortunately, this overlap is not possible in a macroscopic Silicon crystal, but when the

electron and the hole are confined within the small volume of nanocrystals their positions are defined to such a degree that their momenta become undetermined according to one of the basic laws of quantum mechanics, the Heisenberg uncertainty relation. Therefore, the momentum distributions of the electron and the hole get smeared-out and overlap, thus enabling light emission.

Quantum confinement effects describe the modification of material properties of precipitates or clusters depending on their size. It is generally known that the band gap increases with decreasing cluster size. This change is large at visible spectral region and hence small changes in cluster size cause large shifts in energy of the emitted photons. If the emission from the device comes from band to band recombination of excitons in the clusters, the band-gap energy determines directly the energy of emitted photon. The enhancement of radiative recombination rate of excitons with decreasing cluster size is another quantum confinement effect. Because silicon is an indirect band-gap material, generated electron-hole pairs have high lifetimes and they move relatively large distances before recombination. The chance of their combining non-radiatively is high. When the size of the nanoclusters decreases, the number of defects per clusters diminishes. Finally, clusters split to optically active clusters free of defects and optically inactive clusters still containing defects [10]. Reducing the size of a nanocluster also leads to a stronger delocalization of carriers in k-space, and so allows non-phonon assisted transitions [11]. This can be understood when considering Heisenberg uncertainty relations

$$\triangle E \triangle t \geq h, \tag{1.4}$$

$$\triangle p \triangle x \geq h, \tag{1.5}$$

Lifetime of the crystal states is in the range of 10^{-10}-10^{-9}s [11] or more corresponding to the uncertainty in energy E $=10^{-4}$ eV ($h = 4.14 \times 10^{-15} eVs$). With the band-gap energies of $E_g \approx 1$ eV, the energies of states are well defined. When considering the conservation of momentum equation (1.5) can be rewritten in wavevector form as

$$\triangle k \geq \frac{2\pi}{\triangle x}. \tag{1.6}$$

Separation of the conduction band energy minimum from the valence band energy maximum is in the range of $\frac{2\pi}{a}$, where a is a lattice constant ($a \approx 0.5nm$). If we add this to the equation (1.6) and require that the uncertainty of the momentum $\triangle k$ must be greater than this, we obtain equation,

$$\frac{a}{2\triangle x} \approx 1. \tag{1.7}$$

The uncertainty of momentum increases as the size of the nanocrystal decreases and for d= $\triangle$x=0.5 nm the uncertainty of the momentum is as large or larger than $\frac{2\pi}{a}$ which is the minimum position of the conduction band in Silicon allowing non-phonon assisted electron transitions. Phonon assisted and non-phonon assisted processes are assumed to be competitive processes and it is also shown that the probability of non-phonon assisted process reaches the phonon assisted at cluster size of 1mm [11]. It can be derived from molecular orbital theory, that when nanocrystal size decreases tight binding of atoms results in discrete states at the boundaries: at the top of the valence bands and bottom of the conduction bands. The separation of these states and the band-gap increases with decreasing crystalline size. It can be

thus written that

$$E_g \propto d^{-\alpha} \tag{1.8}$$

where E_g is the energy of the gap and emitted photon, d is the diameter of the crystalline and $\alpha \leq 2$ as we mentioned in section 1.2. and figure 1.2.

Quantum confinement is a very attractive emission model due to its simplicity, apparent similarity to the luminescence models from conventional, pn-junction-based LED devices, and because it would introduce an efficient way to control light emission from Silicon-based materials. In reality, the emission model from clusters might be more complicated. Many articles report that the wavelength does not change as the theory predicts and many variations to the quantum confinement theory are proposed. The quantum confinement model will be discussed in relation to the photoexcitation photoemission mechanism models in Si/SiO_2 systems latter in chapter 2.

1.4 Si/SiO_2 Interfaces in $SiO_2/Si/SiO_2$ Multiple Quantum Wells

As described in section 1.3 Silicon based multiple quantum wells and superlattices are engineering solutions to overcome the limitation of bulk crystalline Silicon. A $SiO_2/Si/SiO_2$ single qunatum well is the basic construction block for these set of solution. $SiO_2/Si/SiO_2$ quantum wells have been fabricated by thermal oxidation of SIMOX (Separation by IMplantation of OXygen) Silicon-On-Insulator (SOI) wafer and recently an ELTRAN (Epitaxial Layer TRANsfer) SOI wafer [7]. The interface in the quantum wells, Si/SiO_2 interface is one of the most studied interface,

because of the technological importance of thin Silicon oxide films in semiconductor devices. Gate dielectrics, mask layers, sacrificial layers, insulators, cladding layers in waveguides, etc. are some of the various devices where the properties of the interface between Si/SiO_2 are exploited [12]. When a flat interface between Si and SiO_2 is formed, this is extremely sharp (at a single atom level) and extremely stable with respect to the external agents. For this reason Si nanocrystal embedded in a SiO_2 has been used to form light emitting systems with superior properties with respect to porous Silicon (p-Si). The quality and stability of the Si/SiO_2 interface is what renders this system superior. The structural characterization of Si-nc and of their local environment is fundamental to understand the light emission mechanism in these system. In chapter 2, optical transitions in Si/SiO_2 quantum wells will be discussed.

1.5 Thesis Organization

In this thesis, we study the photoexcitation-photoemission processes in oxidized porous Silicon and nanoscale-Silicon-particle-embedded Silicon oxide system and we verify the use of more than one type of photoluminescence mechanism model used for describing the photoluminescence in this system. For this study the photoluminescence is considered due to photoexcitation and recombination of photo-carriers in nanoscale Si/SiO_2 system, in nanoscale Silicon partcle, in luminescence centers (defects and impurities) in Silicon oxide layers surrounding the nanoscale Silicon particle and in both the nanoscale Silicon particle and luminescence centers.

The thesis is organized into five chapters. Chapter 1 introduces the basics

of optical properties of nanoscale Silicon particle. Chapter 2 discusses the theoretical background for the photoexcitation-photoemission mechanisms in Si/SiO_2 systems and three most fundamental photoluminescence mechanism models, quantum confinment model, surface state model and quantum confinement luminescence center model. Chapter 3 discusses three types of photoexcitation and photoemission processes and we calculate the radiative recombination rates for two of the processes and compare the results obtained. Thus, we give attention to the radiative recombination rates for two types of processes, process A and process B, where in both the photoexcitation and photoemission occur in the nanoscale Silicon particle and the photoexcitation occurs in the nanoscale Silicon particle and the photoemission occurs in the luminescence centers, respectively. Chapter 4 contains the results and discussion of what we obtained in chapter 3, and Chapter 5 gives a summary and conclusion of our work.

Chapter 2

Photoexcitation-Photoemission Process in Si/Si-Oxide Systems

2.1 Introduction

When a porous Silicon (p-Si) is prepared by anodization and put in air it will be oxidized quickly. After 30 minute air exposure, the presence of about 1 to 2% oxygen atoms in p-Si layers was demonstrated [14]. Some freshly prepared p-Si samples may already appear contaminated with oxide, especially when prepared under illumination or by stain etching [13]. Therefore, most porous Silicon studied is oxidized p-Si. Hence, considering that the nanosilicon particle in both oxidized p-Si and the nanosilicon particle embedded Silicon-oxide are covered by Silicon oxide, in this thesis we refer to both of them as nanoscale Si/Silicon-oxide systems.

2.2 Light Emitting Silicon Nanocrystals in SiO_2

Light emitting Silicon dioxide devices are commonly produced by incorporat-

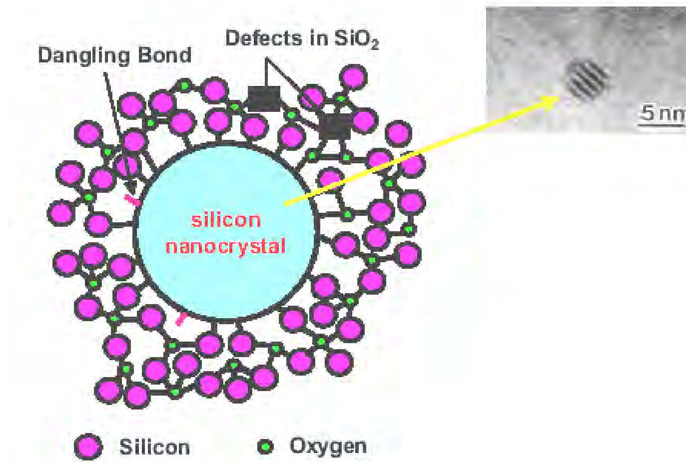

Figure 2.1: Silicon nanocrystals embedded in SiO_2

ing impurity atoms inside the oxide layer by ion implantation, growing Silicon dioxide layers containing Silicon or by growing separate Si/SiO_2 layers (figure 2.1). Light emission properties can be further modified with annealing. Surplus Si^+concentration introduces many kinds of point defects into SiO_2. After annealing, some of these defects become radiative recombination centers or so-called luminescence centers. Luminescence from these radiative defects and nanoclusters is observed in wide visible wavelength range from 460 nm to 950 nm. Different luminescence wavelengths are associated to different luminescence models or point defects in literature. The peaks around 500 nm are explained by radiative electron capture into traps in SiO_2, and quantum confinement in very small Si nanocrystals or excitonic recombination in chains of Si atoms. The peaks around 600-700nm are attributed to electron-hole recombination or unipolar emission from hot electrons in the luminescence center of the SiO_2 near Si nanocrystal-SiO_2 interface [11].

Silicon is not the only dopant from which light emission is obtained. It is known that a small amount of phosphorous in Si nanocrystals enhances the intensity of near IR emission [11]. It is discovered that with phosphorous concentration of 0.1 atomic percentage the light emission efficiency increased and reached the value 2×10^3. It is assumed that the efficiency can be further improved by optimizing the phosphorous concentration. In addition, other group IV elements can be implanted into the SiO_2. C, Ge, Sn can be implanted into SiO_2 and they form nanoclusters during annealing. These impurities emit spectral range from UV to red [10]. Manganese is a yellow $(2.12eV)$ light-emitting centre and it is used in electroluminescent displays. Manganese film was deposited on the Silicon oxide surface and Mn knock-on implantation was used to incorporate Mn impurities to the oxide matrix. Yellow electroluminescence was obtained from Mn implanted samples reaching efficiencies of 1.1×10^{-3} [11]. Erbium ions emit radiation, which is used in optical telecommunications. It is reported that Er in nanocrystal particles containing SiO_2 shows enhanced emission activity [10]. As we mentioned, various dopants can enhance the light emission of SiO_2. However, our motive is to describe how the optical transition process in Si/SiO_2 based nanostructures is possible in the following sections.

2.3 Optical Transitions in Si/SiO_2 Based Nanostructures

Silicon nanostructures such as Quantum Wells (QWs) and superllattices are fabricated with a combination of low band gap and high band gap materials. In the case of Si based QWs and superlattices, the dielectric materials such as SiO_2,CaF_2

and Si_3N_4 have been used as barrier materials. Of all the forms of Si-nanostructures, QWs and superlattices with SiO_2 are the most promising structures for optical device and future memory device, because of their robustness and stability and their full compatibility with main stream CMOS technology. The Si layer thickness in QWs

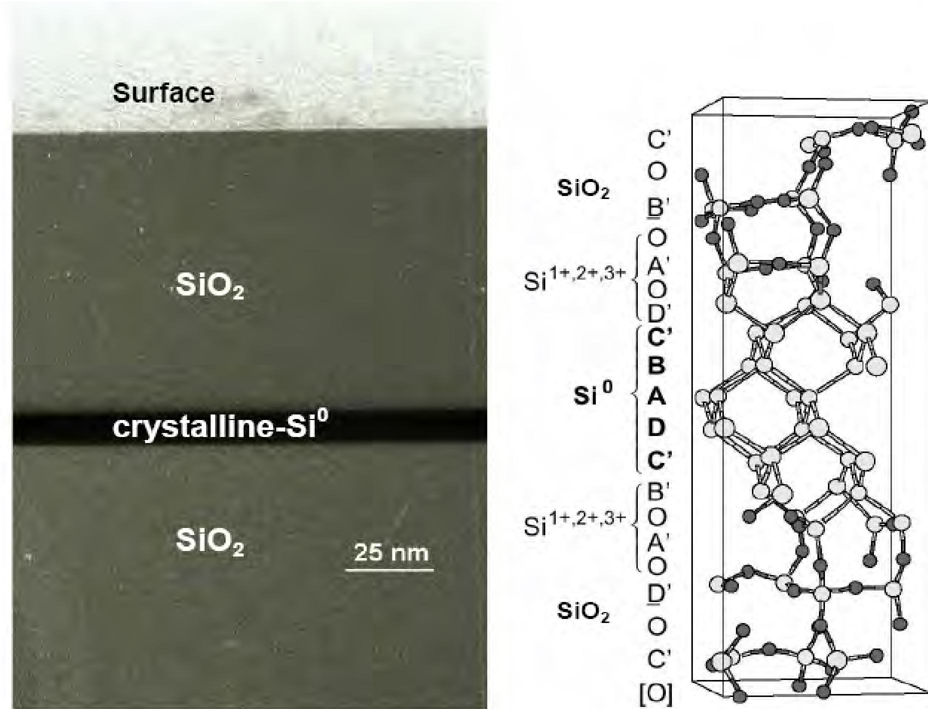

Figure 2.2: Cross section of one SiO_2/Si/SiO_2 QW (left). Side view of Si/SiO_2 SLs model (with 5 bulk-like Si monolayers). The growth axis is the Si-(001) direction in both cases (right) [Lockwood et al].

(Fig.2.2) and superlattices needs to be less than the Bohr radius of bulk Silicon for optical transitions to be observed. The effective Bohr radius of bulk Silicon is expressed in the following equations:

$$a_o = \frac{4\pi\varepsilon\hbar^2}{e^2\mu}, \tag{2.1}$$

where ε the absolute dielectric constant of bulk crystalline Silicon, e is the charge of

an electron and $\hbar$ is the Plank's constant and μ is the reduced mass of Silicon that can be calculated as

$$\frac{1}{\mu}=\frac{1}{m_e}+\frac{1}{m_h}$$

where m_e and m_h are electron and hole mass respectively. The effective Bohr radius of bulk Silicon is a_o =17 Å for $m_e = 1.62m_o$ and $m_h = 0.59m_o$ at $4.2K$ and a_o ≈17 Å at $10K$ for $m_e = 1.06m_o$ and $m_h = 0.59m_o$ and a_o ≈19 Å for $m_e = 0.98m_o$ and $m_h = 0.49m_o$ at $10K$ [7].

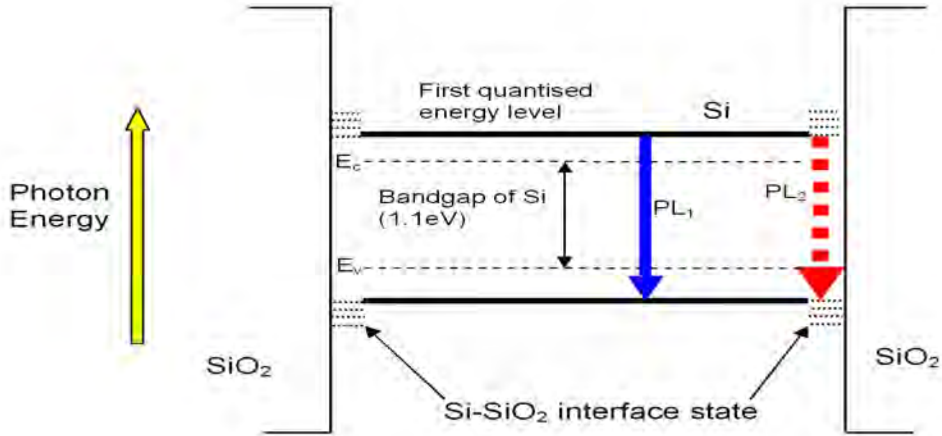

Figure 2.3: Schematic representation of light emmiting mechansim of SiO_2/Si/SiO_2 single quantum wells by (i) quantum confinment (PL_1) depending on Si thickness and (ii) Si-SiO_2 interface (PL_2). Reproduced from ref.[7].

When the Silicon thickness is less than the effective Bohr radius, radiative electron-hole recombination and light emission can be enhanced due to Brillion-Zone folding, described simply when the Si layer thickness along the growth direction is less than the critical thickness, the Brillion-Zone is folded. The conduction band minimum is folded into the Brillion center for $d \approx \frac{5}{2}a$ (a is the lattice constant of

bulk Silicon), which corresponds to 10 layers of silicon for crystalline Silicon [7]. Silicon becomes quasi-direct band gap material and band-to-band transitions should be enhanced for thickness close to the critical thickness. The relaxation of crystal momentum selection rules when electrons and holes are confined to be close together would also be expected to increase radiative transition rates.

Excitation with high energy photons, with higher energy than the quantized energy, results in the creation of e-h pairs in the Si layers of QWs and superlattice. The following two types optical relaxation have been reported, as shown in figure 2.3, the quantum confinement and interface mediated luminescence [7]. Quantum confinement causes thickness dependent shift of luminescent peak energy and is accompanied by a simultaneous luminescent intensity increase for Si/SiO_2 superlattices. Single QWs fabricated by polycrystalline Si deposition and subsequent thermal oxidation have, controversially been reported to exhibit thickness independent luminescence and Silicon dependent quantum confinement [7].

Interface luminescence with weak quantum confinement has been reported for $SiO_2/Si/SiO_2$ single QWs fabricated from SIMOX wafer with ≈ 1.65 eV peak energy [15] and $SiO_2/Si/SiO_2$ single QWs fabricated from ELTRAN wafers with ≈ 1.80 eV peak energy [16]. In p-Si the optical transition results from the combination of the interface state and quantum confinement depending on the size of the cluster. Thus two main mechanisms describe the PL intensities, one unshifted energy peak that is attributed to the interface owing to its observation in all quantum wells while the other shifted energy peaks are attributed to the varying well thickness (i.e, to

confinement). Now let us see how quantum confinement effect in Si/SiO_2 interface is demonstrated and its effect on the optical transition process in the interface.

2.3.1 Quantum Confinement Effect on the Optical Transition in Si/SiO_2 Based Quantum Wells

The confinement effect has first been demonstrated in the theory from the aspect of energy bands that are shown to have absolutely no dispersion in the growth direction axis of the Brillouin zone, corresponding to an infinite effective mass and thus to strong confinement. Additional confined models have also been constructed in order to evaluate the role of suboxides and their oxygen as barriers [17]. All suboxides were shown to form acute barriers, meaning that the wavefunction in the Si well die out exactly right after the interface suboxides Si atoms. On the experimental side confinement has been confirmed from X-ray near edge absorption spectra (XANES).

The energy levels in Si/SiO_2 QWs shown in figure 2.4 are quantized, depending on the Si layer thickness. The well thickness W_1 in the figure is thicker than that of W_2. The emission energy can be adjusted by layer thickness in one dimensional structure (quantum wells and superlattice) and size in the three dimensional structures (quantum dots) covering the entire visible spectrum. As we tried to point out in section 1.2, it is generally accepted that the effective band gap increases because of quantum confinement effect.

The band gap enhancement by quantum confinement can be explained by effective mass approximation [15]. As of the effective mass theory and assuming infinite potential barriers, which is reasonable approximation when wide-gap SiO_2

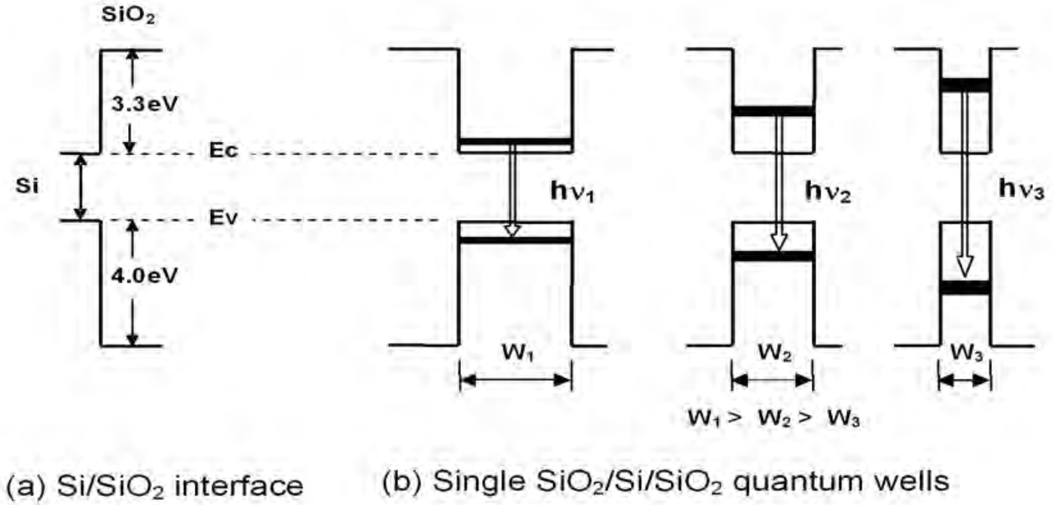

Figure 2.4: Schematic representation of quantum confinement by adjusting the Si layer thickness in $SiO_2/Si/SiO_2$ QWs.

barriers are used, the quantized energy level E_n for one dimensional Si is given by

$$E_n = \frac{1}{2}\left(\frac{\pi n \hbar}{d}\right)^2 \left(\frac{1}{m_e} + \frac{1}{m_h}\right), \tag{2.2}$$

where n =1,2,... is the quantum number of state, and d is the Si thickness along the growth direction. First quantized energy calculated by using equation (2.2) is shown in figure 2.5 when the effective masses $m_e = 1.062m_o$ and $m_h = 0.59m_o$ of crystalline Silicon at $4.2K$ as discussed so far in this chapter.

The variation in PL peak energy with Si layer thickness is shown in figure 2.6 (right) which demonstrates the pronounced blue shift of the PL with decreasing Si layer thickness. As the SiO_2 layer thickness remains constant, the PL can only arise from within the Si layers. This blue shift of the PL and its rapidly increasing intensity with decreasing d is indicative of quantum confinement effect. Lockwood et al [18]

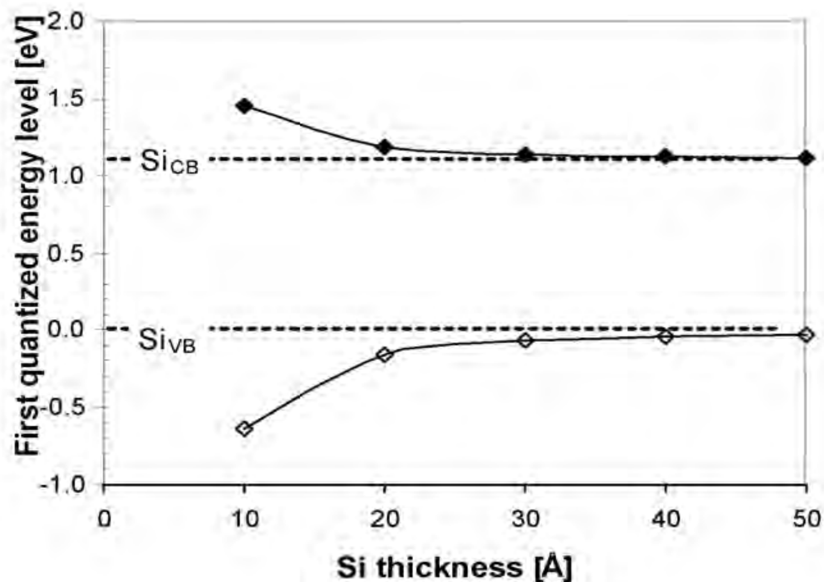

Figure 2.5: First quantized energy level in SiO_2/Si/SiO_2 quantum well, assuming that SiO_2 has an infinite barrier [7].

mentioned in their paper that the visible to near infrared wavelength PL was observed in all superlattices with $d < 3$ nm. A representative 295K spectrum is given in figure 2.6 (left) where the superlattice PL peak is at 1.80 eV (665 nm) with a full width at half maxima of 0.38 eV. The PL peak intensity in the red ($\approx$ 670 nm) wavelength region is comparable to that of the underlaying c-Si substrate Raman peak at 520 cm^{-1}, but the integrated intensity decreases with increasing d (see Fig.2.6(right)) and the PL could not be observed for $d < 3$ nm. The intensity also decreases for $d \leq 1.5$ nm owing to the emitting layers becoming very thin [18].

2.3.2 Interface Mediated Transition

In Si/SiO_2 nanostructures, not only quantum confinement but also Si-SiO_2

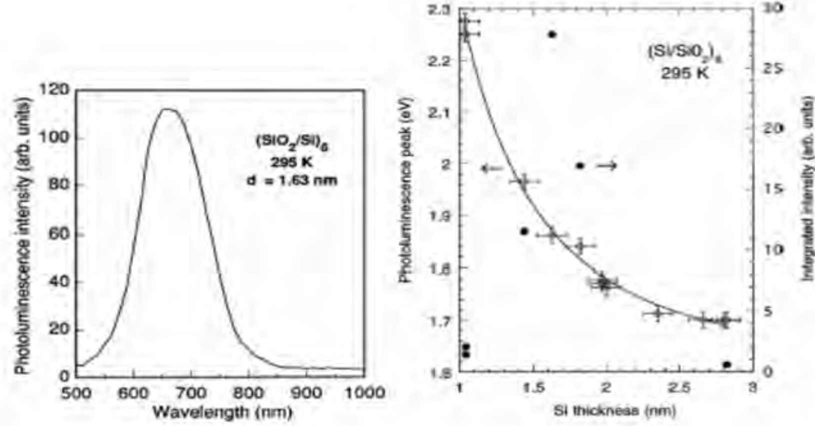

Figure 2.6: Room temperature PL from a Si/SiO_2 superlattice with d = 1.63 nm (right). The PL peak energy (open circles) and integrated intensity (full circles) at room temperature in Si/SiO_2 superlattices as a function of Si layer thickness. The solid line is the fit by effective mass theory [22].

interface states play an important role in the light emission process. In the interface mediated transition process the electrons and holes migrate to the interface where recombination then takes place leading to light emission or PL for p-Si and QWs [15].

The interface oxide could be oxygen deficient silicon oxide, $SiO_x (x < 2)$, or crystalline Silicon oxide or have no chemical and structural transition layer [7]. The double bonded Si=O localized state at the Si / SiO_2 interface of the p-Si trap electrons or holes or both when crystallite sizes are reduced. Recombination via free exciton occurs only for size above 2.8 nm, while the Si=O localized states are involved for smaller crystallites [7]. However the interface luminescence does not follow the expected quantum confinement band gap increase with decreasing crystallite size [16].

2.4 Photoluminescence Mechanism Models

So far we have seen the photoexcitation-photoemission mechanisms in Si/Silicon oxide system and we have discussed the effect of quantum confinement on the optical transitions in these systems. However, there is still much debate about the PL mechanisms of the nanoscale Si/Si oxide systems containing oxidized porous Si and nanoscale-Si-particle (NSP)-embedded Si oxide deposited by chemical vapor deposition, sputtering or Si-ion implanting in to Si oxide. Canham reported strong visible PL from porous silicon at room temperature and suggested the quantum confinement model for its mechanism in 1990 [19]. Since then there has been a long debate on the PL mechanism of p-Si [14]. Some litratures mentioned that more than one type of mechanism models are needed in interpreting PL from p-Si. In the years between 1992 and 1997 there has been at least 24 models different from quantum confinement model suggested [14]. We are not going to address all models, however, we describe the most commonly mentioned PL mechanism models, Quantum Confinement Model (QCM), Surface State Model (SSM), and Quantum Confinement Luminescence Center Model (QCLCM). And we will verify multiple mechanism model in the subsequent chapters by unifying these models. First we discuss them individually.

2.4.1 Quantum Confinement Model

The quantum confinement model (QCM) is the first mechanism model suggested to explain the visible light emission in porous Si. In this model, the light emission process itself was assumed to be the result of carrier recombination within

quantum confined Si-ncs, (i.e.both the optical excitation and recombination takes place inside the nanosilicon particle) and the energies of the resultant PL were expected to inversely scale with the particle size as we have mentioned in section 1.3.1. This is similar to the diagram in figure 2.7 but in this case the emission energy E_g would be replaced by E_{QC}, the energy due to quantum confinement effect, which could be significantly above 1.12eV, due to the quantum confinement of the carriers.

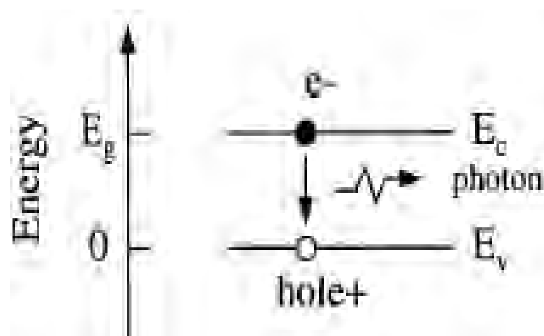

Figure 2.7: Schematic representation of one of the possible optical transitions leading to light emission in semiconductor, band-to-band recombination [20].

Several key factors have been used to support this emission model. These include the presence of intense visible light in Si, the PL blue shift with increased etching, the multi-exponential PL decay characteristics, the 3nm reported particle size, the low temperature Si phonon replicas reported in PL spectrum and the particle size dependent absorption behavior [20]. We will not address all these issues here, however, the following section is devoted to discuss some of these factors along with the shortcomings of the dominant QC model.

Since the report by Canham [19] of an intense red PL from p-Si, calculations have been reported suggesting that the optical gap could lead to sizeable blue shift

due to QC, and oscillator strength would increase significantly, leading to much more efficient PL [20]. In p-Si, Si particle sizes below 5nm would enhance the oscillator strength, as well as produce a sizeable blue shift of optical gap from 1.1eV, possibly in the range of 1.5 to 1.9eV [20]. It was also reported that open circuit etching led to an increase in the porosity of the material, which was interpreted as a reduction in Si particle size [21]. For these types of samples, near IR and visible intense luminescence (800nm to 700nm) was noted, blue shifting toward orange with increased pore widening treatments. This type of pore widening resulted in some samples having particle size as small as 3nm [20].

Further support of the QCM for the emission process has been reported in experiments using resonantly excited PL spectra obtained at liquid He temperatures [20]. Another experimental evidence supporting the QCM is the result obtained from extended x-ray absorption fine structures (EXAFS) experiments [20].

Though several experimental and theorethical evidences supporting QCM are discussed in many literatures concerning the model, it is clear that other interpretations are just as valid. One of the most significant problems with the QCM is that no convincing experimental data exist showing a direct relationship between the PL energy and the particle size in p-Si [20].

As depicted in figure 2.8 Kanemaitsu et al.[22] have examined the relationship between particle size and PL peak energy in p-Si, using optical absorption, Raman spectroscopy and photoluminescence. They reported results from samples corresponding to 2nm, 3.5nm, 9nm and 13nm particle sizes, where a blueshift in op-

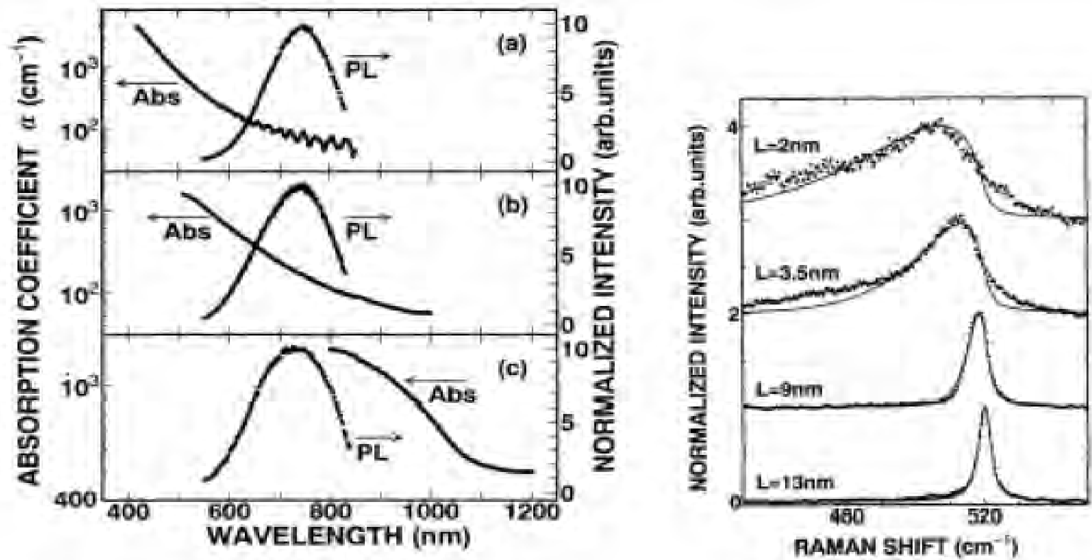

Figure 2.8: Typical absorption and PL spectra of p-Si films (a) L= 2nm, (b) L =3.5nm, and (c) L= 9nm (left). Raman spectra of free standing p-Si films compared with the spectra calculated for a sphere of dimeter L (solid lines) (right) [22].

tical absorption was noted with decreasing particle sizes, but no shift in the red PL peak energy was not ever noted. There results have shown quite conclusively that the PL peak emission energy is not correlated to the particle size, which contradicts the QC picture. Different results of their work are shown in figure 2.8.

With the above results at least, alternate models involving mechanisms other than Si nanoparticle emission must be considered in order to determine the origin of the PL.

2.4.2 Surface State Model

From an optical emitter, the quantum efficiency is defined as the probablity of radiateive recombination following excitation. The efficiency of Si-ncs, which can decay through radiative decay rate to the total decay rate, as described in section

1.3.1 QC leads to an enhancement in the radiative rate.In systems of Si-ncs, one can

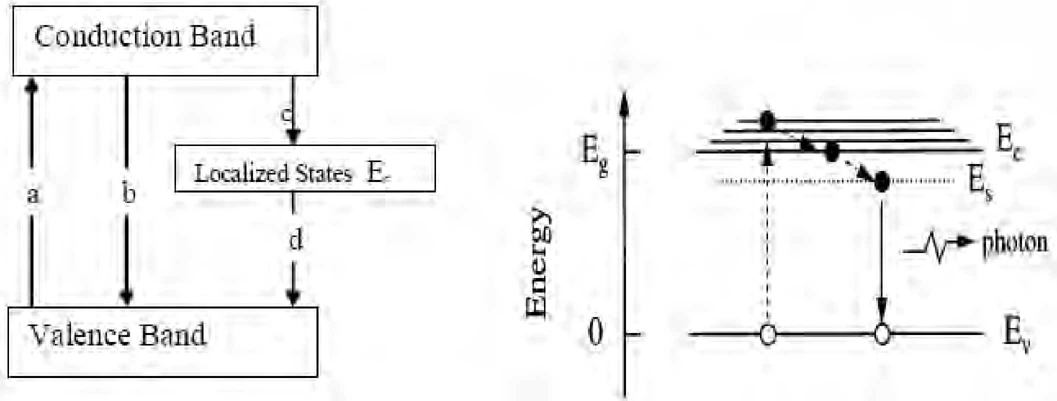

Figure 2.9: Schematic of possible excitonic recombination paths (a) excitation: excited states (valence band) to excited states (conduction band); (b) dexcitation: conduction to valence band recombination; (c) relaxation: excited states to localized surface states (LSS) and (d) radiative recombination: LSS to ground states (left) [21]. Intrinsic surface state emission process (right) [20].

additionally take advantage of the high quality oxide to passivate the surface and therefore, eliminate many nonradiative channels, such as dangling bonds and defect centers. This further enhances the quantum efficency by reducing the total decay rate.

However, the effect of Si-nc surface structure can't be neglected, Ghoshal et al.[8]. Indeed, despite the predicted essentialy d^{-2} dependence of the nanocrystals band gap in equation (1.1), several experimental studies have indiacted that, altough the PL of Si is indeed blue shifted as its dimension decreases, the shift is smaller than expected [21]. In addition, a relatively wide range of experimental PL measurments for small Si nanocrystals have been reported in literature [4, 15, 17, 21].

In the majority of systems that have been investigated, the Si-ncs are coor-

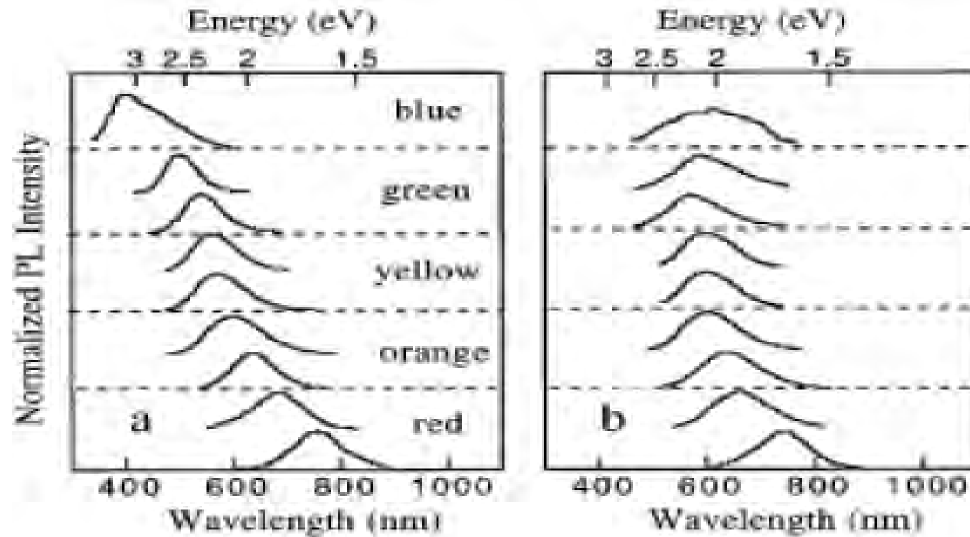

Figure 2.10: Room temperature PL spectra from p-Si samples with different porosities kept under Ar atmosphere (a) and after exposure to air (b).

dinated to oxygen at the surface, either because they are syntesized within a SiO_2 matrix or due to the rapid native oxidation of Si surfaces in an arobic environment as we mentioned in the introduction of this chapter. It is therefore difficult to separate the role of these surface groups from the intrinsic properties of the nanocrystals. Islam et al.[23] suggested a theorethical surface state model that accounts for localized states at the surface of the Si-ncs. In this model, they developed an analytical expression to compute the PL, combining the QC effect specifically, they consider (a) gap widening due to QCE (b) the oscillator strength, (c) exciton binding energy and (d) localized surface states. As these factors depend on both the crystallite sizes and their dispersion. Furthermore, they mentioned that, the surrounding medium also affects the surface states.

The above mentioned model is able to predict PL peak position and line

shape with respect to mean crystallite size and its dispersion. Figure 2.9(left) shows various possible electronic transition during PL emission from nanocrystallites. On excitation with high energy photons photocarriers are generated inside the crystallites (path a) and then a fraction of these photoexcited carriers relax nonradiatively to the surface states (path c). Subsequently, the relaxed carriers recombine to ground state radiatively giving PL (path d). Figure 2.9 (right) shows the emission process due to the intrinsic surface state.

In general the analytical expression that Islam et al. developed in their work on surface state model by unifying the quantum confinment effect and the localized surface states was helpful in describing the experimental PL spectra from Si-ncs. Furtheremore, the role of surface states, especially for low crystallite size, has been clearly demonstrated and explicitly included in PL model. Thus, we can say that the model is useful in understanding the role of surface passivation and surrounding media on the PL process in Si-nc which were not included in the QCM (figure 2.10).

2.4.3 The Quantum Confinment Luminescence Center Model

The quantum confinement model of porous Si which assumes that both the optical excitation and recombination take place inside the nanoscale Silicon particle (NSP), and the energy gap of the particle is enlarged due to the quantum confinement effect, can explain the emission photon energy of PL in the range of visible light and supported by experiments as we mentioned in section 2.4.1. Based on this model a new model, QCLCM was suggested by Qin and Jia in 1996 [24]. The main point of view of this model is that the quantum confinement of carriers does take place in

the NSP, which causes the optical excitation in an energy rage to be much higher than that of the bulk Si band gap and the photoexcitation photoemission process can occur outside the NSP. The following four points were noted in the model; (1). In NSP, photoexcitation creates e-h pairs where the energy of a pair is much larger than the bandgap of bulk Si. (2). The probability of the radiative recombination inside the NSP is negligible in comparison with that outside the NSP. The surface region of NSP can be case (I) covered by SiO_2 layer, case (II) not covered by SiO_2.

It was also assumed that the recombination of e-h pair produced in a NSP to emit visible light to be through various luminescence centers (point defects or impurities), which are located at the Si/SiO_2 interfaces and/or in the thin SiO_2 layers and/or on its outer surfaces in case I. As for case II, the Luminescence centers are located on the surfaces of NSPs. Figure 2.11 shows schematically the radiative recombination process for case I where the carriers may enter the SiO_2 through the tunneling effect and recombine at the luminescence centers to emit light. (3). The nonradiative recombination (NRR) of e-h pairs is negligible inside the NSP but takes place in case I at the Si/SiO_2 interface and /or in the SiO_2 layers and/or at the outside surfaces of SiO_2, and in case II on the surface of NSP. (4). Strong stress at the Si/SiO_2 interfaces or on the surfaces of NSP can modify the electronic structure of the luminescence centers located there and thus the PL band enegy. The thickness, density, structure and stoichiometric composition devation of the SiO_2 layer can also affect the electronic structure of the luminescence centers in SiO_2 or on its outer surface or at the Si/SiO_2 interface. This model is supported by various arguments [22].

However, we would not mention these arguments here, we rather want to highlight some interpretations of few experimental results of the PL in p-Si using this model made by Qin and Jia.

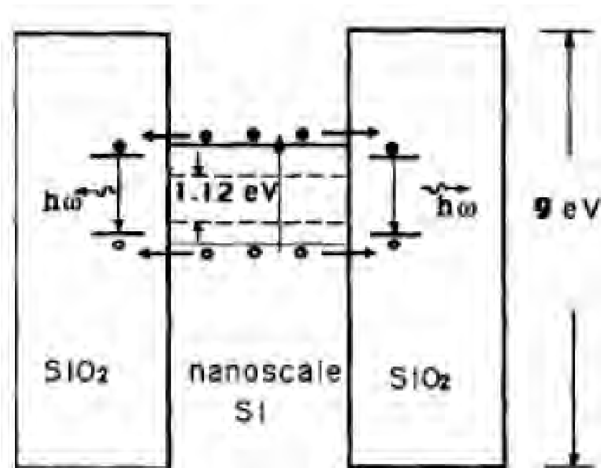

Figure 2.11: Schematic illustration of electron-hole pairs recombining to emit visible light through luminescence centers, which are located in the SiO_2 layers,. a situation of case I [24].

(1) As shown in figure 2.11, e-h pairs inside the NSPs with sufficient energy and density are excited by laser and this is a prerequiste for the emission of visible light. The e-h pairs recombine outside the NSP through the luminescence centers (LCs) whose energy level positions are suitable for visible light emission. In this way one can explain the visible PL in p-Si. It can be seen from the figure that the energy gap in NSP which is enhanced by the QC effect is larger than the PL emission energy. (2) In the model, the high quantum efficiency of the PL in p-Si can be attributed to (a) the efficiency of radiative recombination through LCs outside NSP is much higher than that trough band to band recombination inside NSP and the latter is near to or some what higher than band to band transition in bulk Si, and (b) the probablity

of NRR in NSP is much lower than that in bulk Si as discussed in (1). (3) It is easy to explain the multi-peak structure in PL and electroluminescence[1] spectra, if we assume that more than one kind of LCs are responsible for the PL. (4) Because the PL energy in this model is determined directly by the energy levels of the LCs outside the NSP, one can't expect a PL blueshift by only increasing the porosity of the p-Si sample. (5) The experimental PL peak position has generally been found in the wavelength range of 560-800nm. As of this model, this PL range is determined by the available LC in p-Si samples.

Thus, we can say that the main points of this model are that the QC of carriers in the nanosilicon causes the optical transition in an energy range much higher than the bandgap of bulk Si and that the radiative recombination of carriers are realized through the LCs outside the NSP. The lack of nonradiative recombination centers inside NSP and good passivation of their surfaces by H or O results in a much smaller nonradiative recombination probability in p-Si than bulk Si and in higher radiative recombination probablity through LCs than through the indirect band to band transition in bulk Si, these are the two main reasons why PL in p-Si is much stronger than in bulk Si.

Keeping these arguments in mind however we would like to give a systematic description to calculate some relevant quantities that possibly explain the mechanism of photoluminescence.

---

[1] Electroluminescence is an optical process where light is generated by current injection into the Si-nc

Chapter 3

Mechanism Model for Recombination Rates in Si/Si-Oxide Systems

3.1 Introduction

So far we have discussed the basics of few but fundamentals of the photoluminescence mechanism models, QCM, SSM and QCLCM. As we mentioned in chapter 2, in order to describe the photoluminescence mechanism to understand the spectra in porous Silicon the contributions of more than one models are important. In this chapter, since the PL in p-Si is dependent on the radiative recombination rate, we calculate the rate for three different types of emission process which are associated with the mechanism models, QCM and QCLCM. We also discuss how the radiative recombination rate depends on the size of the nanosilicon particle. Finally we would predict the domination of either of the models in describing the PL from p-Si in the given size and oxidation limit.

Based on the QC and QCLC models we consider three types of photoex-

citation -photoemission processes for e-h pairs in the photoluminescence of porous Silicon: process A, B and C. Each of them includes both radiative and nonradiative processes.

In process (A) both the photoexcitation and photoemission processes occur in the NSPs, as described in the QCM.

In process (B) photexcitation occurs in the NSPs and photoemission occurs in LCs in Silicon oxide adjacent to the NSPs. As QCLCM claimed that the photexcitation of e-h pairs occurs mainly in the NSP and photoexcited e-h pairs tunnel into the LCs in the surrounding medium, which in our case is the SiO_2, and then radiatively recombine there, this emission process can be said the emission process in QCLCM.

In process (C) both photoexcitation and photoemission occur in LCs in SiO_2. This process highly depends on the LCs density in the system.

Now, lets consider the three types of processes in the PL from a strong light emitting nanosilicon/Silicon-oxide system as described above. The recombination rates of e-h pairs in processes A, B and C are referred to as P_a, P_b and P_c while radiative recombination rates of e-h pairs in process A, B and C as P_{ar}, P_{br} and P_{cr}, respectively. We have,

$$P_{ar}=\frac{N_{eh}}{\tau_{ar}} \text{ and } P_{br}=\frac{N_{eh}}{\tau_{br}} \ . \tag{3.1}$$

Here N_{eh} is the density of the e-h pairs in NSPs, and τ_{ar} and τ_{br} are radiative recombination life times in processes A and B, respectively.

3.2 Radiative Recombination Rate for the QCM Process

As we mentioned in the introduction of this chapter, QCM claimed that both the photoexcitation and recombination of photo-carriers occur in the nanoscale silicon particle. So in order to calculate the radiative recombination rate for the QCM process we consider the photoexcitaion-photoemission process as in process A.

Suppose that all NSPs in the Si/SiO_2 system are cubes with the same size L and using effective mass and deep well approximation[1], the following result for radiative recombination rate for recombination of e-h pairs in the nanosilicon particle, as in process A was obtained [13].

$$\frac{1}{\tau_{ar}} = \beta \frac{E_o(L)\sin^2(k_oL/2)}{\left[k_o^2 - (2\pi/L)^2\right]^2 L^6} , \tag{3.2}$$

where

$$\beta = \frac{512\pi^4 e^2 n(\left|p_{cv}\right|^2/2m)}{3m\hbar^2 c^3 k_o^2} ,$$

$E_o(L)$ is the energy, the transition energy obtained by considering the quantum confined charge carriers in a three dimensional box of side length L.

$$E_o(L) = E_g + \frac{\hbar^2}{2m}\left[\frac{1m}{m_l} + \frac{2m}{m_t} + \frac{3m}{m_h}\right]\left(\frac{2\pi}{L}\right)^2 ,$$

$k_o = 0.85 \times 2\pi/a$ ($a = 5.43\,\text{Å}$ is the lattice constant) is the Si conduction band minima in ΓX direction [25], n is the refractive index of bulk Si, e is the charge of an electron, m is the mass of an electron, c is the speed of light, p_{cv} is the dipole matrix element for vertical transition in bulk Silicon, E_g is the forbidden gap for bulk Si, m_l and m_t

[1] The infinite potntial barrier approximation taken is reasonable since the potential well depths for electrons and holes are 3.2 and 4.6 eV which are wide enough for the approximation to be valid [25].

are longitudinal and transverse effective masses for electron in Si, respectively, and m_h is the effective mass for holes in Si.

3.3 Radiative Recombination Rate for the QCLCM Process

In order to calculate the radiative recombination rate for the QCLCM, $1/\tau_{br}$, we suppose that the x, y, and z axis are located along the three sides of the cubic NSP as shown in figure 3.1(a). When we consider the tunneling of electrons along the z direction, the barriers of SiO_2 are considered infinitely deep along the x and y direction while of the actual depth along the z direction. Therefore, the electrons and holes photoexcited in the NSP can only tunnel through the barriers along the z direction [12, 13, 26]. Figure 3.1(b) shows the z-direction electron potential with a SiO_2 layer thickness d surrounding a NSP and a LC as shown in (a). It is assumed that the LC has a negative δ potential, which is,

$$\begin{aligned} U_{LC} &= -U,\ \xi-\varepsilon \leq z \leq \xi+\varepsilon \\ &= 0,\ \text{otherwise} \quad . \end{aligned} \tag{3.3}$$

Recalling a relation from the Kroning-Penny model, when U_1 and ε tend to infinity and zero simultaneously, $2\varepsilon U_1$ remains a constant. The rate for a carrier (an electron or a hole) in a NSP to hit the SiO_2 barrier at +z or -z direction is $p_z/2m_zL$, where m_z and p_z are the effective mass and momentum of the carrier in the z direction, respectively. Because the height of the barrier for electron U_{oe} and m_z are smaller than those for a hole, respectively the tunneling current for electrons is evidently greater than that for holes. The charges accumulated will cause electric field, which

enhances the hole current and depresses the electron current, and results in equal currents in a stationary state.

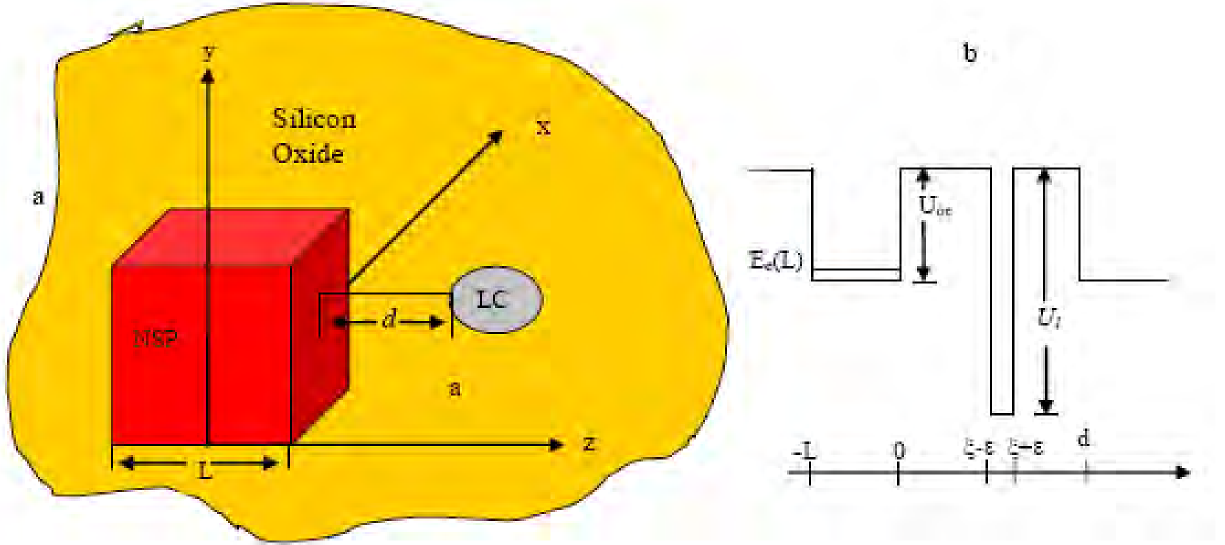

Figure 3.1: (a) Our schematic drawing of the QCLCM. The NSP and a LC are simplified as a cubic quantum box of side L and a small sphere. (b) The z-direction electron potential of a SiO_2 layer of thickness d adjacent to the NSP with side length L and of a LC located in the SiO_2 layer.

It is further considered that after the photoexcitation the carriers in the NSP relax to the ground state before tunneling. As soon as an electron entering the excited electron state of a LC, the lattice will relax to the thermal equilibrium configuration for excited electron state by emitting multiphonons.

Here we want to illustrate where the carriers are going after entering the LC, a drawing of energy structure of a LC is plotted in figure 3.2. Where the horizontal axis is the configurational coordinate of the lattice vibration, the vertical is the total energy of the electron and the lattice, and U_i and U_j are the total energies of electron and the lattice as a function of configurational position where the electron is in the

bound state I and J respectively.After the tunneling of e-h pair into the barrier and

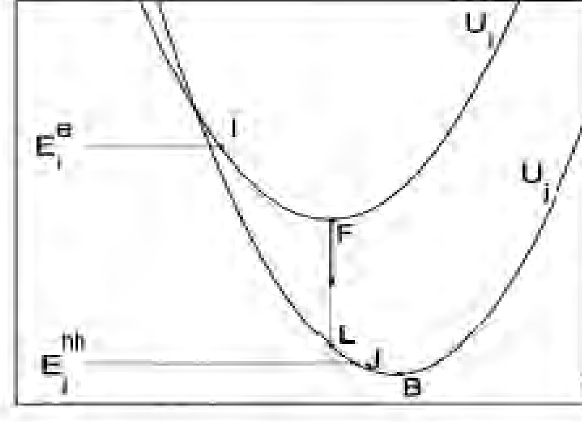

Figure 3.2: Energy diagram of a LC.

being captured by the LC, which has the same energies as the electron had before tunneling, then it relaxes to the lowest energy state F (at the equilibrium position of the lattice vibration) by emitting multiphonons. Meanwhile the hole enters the energy state J, then relaxes to the state L. Once the electron reaches the state F and the hole, the state L, generally they can't tunnel back to the nanosilicon box because there are no states which have the same energy as the states F and L to accept them. However, they can recombine radiatively to emit visible light. The energy difference between the electron state F and the hole state L, $E_{phot} = E_F - E_L$ is the photon energy emitted from the LC, to do so the necessary condition for LC's emitting photons with energy

$$E_{phot} \leq \triangle E_{IJ} \ . \tag{3.4}$$

Where $\triangle E_{IJ} = E_I^e - E_J^h$ is the transition energy (cf. Eqn. 3.2). The electron-hole pair in the LC recombine radiatively with $1/\tau_{br}$ given below [14].

$$\frac{1}{\tau_{br}} = (V_e \sigma_e^o + V_h \sigma_h^o) N_{LC} \eta_{LC} \quad , \tag{3.5}$$

with σ_e^o and σ_h^o are the capture cross-sections for a neutral LC.

Here it is important to note that the capture cross-sections depend on the charged state of the LCs and which are mainly determined by the photon emission process and are approximately independent of the initial energy of the electron in NSP. Assume that the LCs are uniformly distributed in the SiO_2 layer and are neutral before illumination, both an electron and a hole can be captured by a neutral LC with capture cross-sections σ_e^o and σ_h^o, then the LCs changes to be negative and positive respectively. Then a hole and an electron can be captured by the negative and positive LCs, respectively with large capture cross-sections.

The V_e and V_h in equation (3.5) are the effective velocities (equivalently the mobilities) of electron and hole in the SiO_2 layer and given by [14],

$$V_e = \frac{\pi^3 \hbar^3}{4 U_{oe} L^4} \left(\frac{1}{m_l} + \frac{2}{m_t} \right) \left[\frac{1}{m_l k_{el}} \left[1 - e^{-2k_{el} d} \right] + \frac{2}{m_t k_{et}} \left[1 - e^{-2k_{et} d} \right] \right], \tag{3.6}$$

$$V_h = \frac{9 \pi^3 \hbar^3}{4 U_{oh} L^4 m_h^2 k_h} \left[1 - e^{-2k_h d} \right] \ . \tag{3.7}$$

where k_{el}, k_{et}, and k_h are obtained by solving the Shrodinger equation for the elctron and hole in the SiO_2 layer with respective energy eigenvalues, $E_e(L)$ and $E_h(L)$,

$$k_{el} = \frac{[2 m_l (U_{oe} - E_e(L)]^{1/2}}{\hbar} \text{ and } k_{et} = \frac{[2 m_t (U_{oe} - E_e(L)]^{1/2}}{\hbar}, \tag{3.8}$$

$$k_h = \frac{[2m_h(U_{oh} - E_h(L)]^{1/2}}{\hbar}, \tag{3.9}$$

and

$$E_e(L) = \frac{\pi^2\hbar^2}{2L^2}\left(\frac{1}{m_l} + \frac{2}{m_t}\right) \text{ and } E_h(L) = \frac{3\pi^2\hbar^2}{2m_h L^2}. \tag{3.10}$$

In equation (3.5) N_{LC} is the density of the LCs in the system and η_{LC} is the PL efficiency of the LC, U_{oh} and U_{oe} are the heights of the barrier for holes and electrons in SiO_2 layer, d is the thickness of the SiO_2 layer, and $E_e(L)$ and $E_h(L)$ are the energies of an electron and a hole in a NSP in their ground states respectively.

Because the thickness of the SiO_2 layer is usually larger than the thickness of a molecular layer of oxide of about 0.3-0.4nm [13, 14], the factors $e^{-2k_{et}d}$, $e^{-2k_{el}d}$ and $e^{-2k_h d}$ are much smaller than 1 and can be neglected. Then the expression for V_e and V_h can be rewritten as,

$$V_e = \frac{\pi^3\hbar^4}{4\sqrt{2}}\left(\frac{1}{m_l} + \frac{2}{m_t}\right)\left(\frac{1}{m_l^{3/2}} + \frac{2}{m_t^{3/2}}\right)\frac{1}{U_{oe}\left[U_{oe} - E_e(L)\right]^{1/2} L^4}, \tag{3.11}$$

$$V_h = \frac{9\pi^3\hbar^4}{4\sqrt{2}}\left(\frac{1}{m_h^{5/2}}\right)\frac{1}{U_{oh}[U_{oh} - E_h(L)]^{1/2} L^4}. \tag{3.12}$$

3.3.1 Limiting Cases

We want to impose two limiting cases for the capture cross-sections and see what happens to equation (3.5).

Case I: If the LCs are neutral and $\sigma_e^o >> \sigma_h^o$, or when the LCs are charged

negatively before illumination. We have,

$$\begin{aligned}\frac{1}{\tau_{br}} &= \left(V_e\sigma_e^o + V_h\sigma_h^o\right) N_{LC}\eta_{LC} \\ &= \left(V_e + V_h(\frac{\sigma_h^o}{\sigma_e^o} \approx 0)\right) \sigma_e^o N_{LC}\eta_{LC} \\ &= V_e\sigma_e^o N_{LC}\eta_{LC}.\end{aligned}$$

Substituting equation (3.11), we have,

$$\frac{1}{\tau_{br}}= \alpha_e \frac{\sigma_e^o N_{Lc}\eta_{LC}}{\left[U_{oe} - E_e(l)\right]^{1/2} L^4}, \tag{3.13}$$

where,

$$\alpha_e = \frac{\pi^3\hbar^4}{4\sqrt{2}}\left(\frac{1}{m_l} + \frac{2}{m_t}\right)\left(\frac{1}{m_l^{3/2}} + \frac{2}{m_t^{3/2}}\right)\frac{1}{U_{oe}},$$

is a constant independent of the size of the NSPs and the parameters of the LCs.

Case II: If the LCs are neutral and $\sigma_h^o >> \sigma_e^o$, or when the LCs are positively charged before illumination. We have,

$$\begin{aligned}\frac{1}{\tau_{br}} &= \left(V_e\sigma_e^o + V_h\sigma_h^o\right) N_{LC}\eta_{LC} \\ &= \left(V_e(\frac{\sigma_e^o}{\sigma_h^o} \approx 0) + V_h\right) \sigma_h^o N_{LC}\eta_{LC} \\ &= V_h\sigma_h^o N_{LC}\eta_{LC}.\end{aligned}$$

Substituting equation (3.12) yield,

$$\frac{1}{\tau_{br}}= \alpha_h \frac{\sigma_h^o N_{LC}\eta_{LC}}{\left[U_{oh} - E_h(l)\right]^{1/2} L^4}, \tag{3.14}$$

where,

$$\alpha_h=\frac{9\pi^3\hbar^4}{4\sqrt{2}}\left(\frac{1}{m_h^{5/2}}\right)\frac{1}{U_{oh}},$$

is a constant independent of the size of the NSPs and the parameters of the LCs. In actual nanoscale Si/SiO_2 system, the sizes of NSPs are not uniform and have a distribution, usually the Gaussian one [21]. We take

$$\varphi(L) = \frac{1}{\sigma\sqrt{2\pi}} \exp\left[-\frac{(L-L_m)^2}{2\sigma^2}\right]. \tag{3.15}$$

Here L_m and σ are the mean crystallite size and standard deviation, respectively, for the NSP ensemble. Assuming that the sizes for the NSPs have a lower limit, which is denoted by L_o, we have the following two expressions for the average values of $1/\tau_{ar}$ and $1/\tau_{br}$ over the nanoscale Si/SiO_2 system,

$$\begin{aligned} \langle\frac{1}{\tau_{ar}}\rangle &= \int_{L_o}^{\infty} \frac{1}{\tau_{ar}}\varphi(L)dL, \qquad (3.16) \\ &= \frac{\beta}{\sigma\sqrt{2\pi}} \int_{L_o}^{\infty} \frac{E_o(L)\sin^2(k_oL/2)}{\left[k_o^2-(2\pi/L)^2\right]^2 L^6} \exp\left[-\frac{(L-L_m)^2}{2\sigma^2}\right] dL, \end{aligned}$$

and

$$\begin{aligned} \langle\frac{1}{\tau_{br}}\rangle &= \int_{L_o}^{\infty} \frac{1}{\tau_{br}}\varphi(L)dL, \qquad (3.17) \\ &= \frac{\alpha_{h/e}}{\sigma\sqrt{2\pi}} \int_{L_o}^{\infty} \frac{\sigma^o_{h/e}N_{LC}\eta_{LC}}{\left[U_{oh/e}-E_{h/e}(L)\right]^{1/2} L^4} \exp\left[-\frac{(L-L_m)^2}{2\sigma^2}\right] dL. \end{aligned}$$

Here h/e in subscript indicates that the expresion is either for electron or hole.

3.4 The Critical Luminescence Center Density

Now, since the rates $1/\tau_{ar}$ and $1/\tau_{br}$ calculated in the previous section represent the rates of two processes, the process A, and the process B, by comparing the two expressions, $\langle 1/\tau_{ar}\rangle$ and $\langle 1/\tau_{br}\rangle$, we can determine the importance of either of the processes in the given range of size of the particle.

To do so, we need to calculate the critical density of LCs, N_{LC}^{crit} at which the two processes can explain the PL mechanism of Si/SiO_2 system equally. Thus, for a given capture cross-section, say in case I, when $N_{LC} > N_{LC}^{crit}$, we have, $\langle\frac{1}{\tau_{br}}\rangle > \langle\frac{1}{\tau_{ar}}\rangle$, for $N_{LC} < N_{LC}^{crit}$, we have $\langle\frac{1}{\tau_{ar}}\rangle > \langle\frac{1}{\tau_{br}}\rangle$, and when $N_{LC} = N_{LC}^{crit}$, we get,

$$\langle\frac{1}{\tau_{ar}}\rangle = \langle\frac{1}{\tau_{br}}\rangle \ . \tag{3.18}$$

Using the equations (3.16) and (3.17), we can find the following expressions for N_{LC}^{crit}, when the capture cross-section is taken to be as in case I.

$$N_{LC}^{crit} = \frac{\beta}{\alpha_e \eta_{LC} \sigma_e^o} \times \frac{\int\limits_{L_o}^{\infty} \frac{E_o(L)\sin^2(k_o L/2)}{[k_o^2 - (2\pi/L)^2]^2 L^6} \exp\left[-\frac{(L-L_m)^2}{2\sigma^2}\right] dL}{\int\limits_{L_o}^{\infty} \frac{1}{[U_{oe} - E_e(L)]^{1/2} L^4} \exp\left[-\frac{(L-L_m)^2}{2\sigma^2}\right] dL} . \tag{3.19}$$

We can find a simplified form of the above equation by using the following two approximations:

(1). The term $\sin^2(k_o L/2)$ in equation (3.1) is a fast vibrational function of L with a period of $a/0.85$ nm, and for the nanoscale Si/SiO_2 system, the full width of half maxima for NSP size distributions are of $2(2\ln 2)^{1/2}\sigma = 2.35\sigma$ which is usually larger than $a/0.85$ nm. So instead of taking $\sin^2(k_o L/2)$ its average value $1/2$ can be used approximately.

(2). The L in equation (3.2), (3.6) and (3.7) is substituted by its most probable size L_m. Then we have the following equations,

$$\langle\frac{1}{\tau_{ar}}\rangle = \beta \frac{E_o(L_m)}{2\left[k_o^2 - (2\pi/L_m)^2\right]^2 L_m^6} . \tag{3.20}$$

When the LCs are neutral and $\sigma_e^o >> \sigma_h^o$ or when the LCs are negatively charged before illumination. Again

$$\langle\frac{1}{\tau_{br}}\rangle = \alpha_e \frac{\sigma_e^o N_{LC} \eta_{LC}}{[U_{oe} - E_e(L_m)]^{1/2} L_m^4}. \tag{3.21}$$

When the LCs are neutral and $\sigma_h^o >> \sigma_e^o$, or when the LCs are positively charged before illumination the subscripts "e" in equation (3.21) should be substituted by "h".

From equations (3.18), (3.20) and (3.21) when the LCs are neutral and $\sigma_e^o >> \sigma_h^o$, or when the LCs are negatively charged before illumination, we have,

$$N_{LC}^{crit} = \frac{\beta E_o(L_m) [U_{oe} - E_e(L_m)]^{1/2}}{2\alpha_e \sigma_e^o \eta_{LC} \left[k_o^2 - (2\pi/L_m)^2\right]^2 L_m^2} \tag{3.22}$$

3.5 Radiative Recombination Rate for the LC Process

We believe, the model calculations above would give good insight to the radiative recombination rates for the two kind of processes, process A and process B. We now therefore want to put a sort of theoretical relation to the radiative recombination rate of process C. As we mentioned at the beginning of this chapter, the radiative recombination rate in process C is proportional to the LC density in the system as both the photoexcitation and photoemission of e-h pair take place in the LCs in this type of process. So for the more defect or impurities we have in the sample the process is more important. And for that of process A, the radiative recombination rate is proportional to the NSP. So, we can have the following relation,

$$\frac{P_{cr}}{P_{ar}} \approx \frac{N_{LC} \sigma_{LC} \eta_{LC}}{N_{NSP} \sigma_{NSP} \eta_{NSP}} \tag{3.23}$$

where N_{NSP} is the density of the NSP; η_{LC} and η_{NSP} are the luminescence efficiencies of LC and NSP, σ_{NSP} and σ_{LC} the capture cross-section of a LC and a NSP. On the basis of these expressions, we present our results in the next chapter.

Chapter 4

Results and Discussions

4.1 Photoluminescence Mechanism

In this chapter, we present the main results that we obtained based on model calculation in chapter 3.We also discuss the importance of more than one mechanism models to describe the PL spectral profile in oxidized porous Silicon and nanoscale Silicon particle embedded Silicon oxide system. The plots are generated from the relation we obtatin in equations (3.2), (3.13), (3.22) and (3.23). Finally, we clearly verify the importance and need of multiple mechanism model to describe the PL mechanism in oxidizd p-Si.

In order to obtain an insight of the effect of size on the radiative recombination rates and hence on the PL spectral profile of the system, two models are considered, the quantum confinement (QC) and quantum confinement luminescence center (QCLC) models. Three types of competitive photoexcitation-photoemission processes, processes A, B and C. The first two are associatd with the models we used, respectively. The PL emission is observed when optical transitions occurred as we

mentioned in chapter 2. The photoexcitation is due to the illumination of light, and the photoemission occurs when the photocarriers (e-h) recombine. The electron hole recombination time (life time of exciton) is strongly related to the particle size as seen from the expressions. The radiative recombination is most important property in connection with the photoemission efficiency and quantum yield. If the radiative recombination rate is relatively high, a pair comprised an excited electron and hole can recombine via radiative emission process, the emission process which releases photons. If the radiative recombination rate is low, on the other hand non-radiative recombination events degrade the performance of light emission as a rusult no visible luminescence is observed.

Since we considered oxidized p-Si and nanosilicon particle embedded Silicon-oxide in our study, the recombination of the excited photocarriers may occur either in the nanosilicon particle or LCs (defects and impurities) in the SiO_2 layer surrounding the NSP.

Different authors in different literatures predicted that measuring the PL peak energy as a function of the size of the nanosilicon particle is an important experimental method to check the PL mechanism model [27]. If the PL peak energy shifting with the nanosilicon particle sizes just consistent with what the QC effect predicts the QCM is verified. If the PL peak energy pins nearly at a fixed energy independent on the NSPs, the QCLCM is verified. Inspite of the above explanation there is no systematic and clear description of PL mechanism model therefore, we followed a different procedure to verify the multiple mechanism model for the PL

from the system considered and our results are in conformity with other observations.

4.2 Radiative Recombination Rate

We used the radiative recombination rates for both the QCM and QCLCM processes as in equation (3.2) and (3.13). The expressions for radiative recombination rates of processes A and B roughly vary as L^{-6} and L^{-4}, respectively. We can see that as L increases, $1/\tau_{ar}$ and $1/\tau_{ar}$ decreases with the indicated power of L. However, for a given size of the system, for smaller sizes of NSP, the radiative recombination rate $1/\tau_{ar}$ is greater than $1/\tau_{br}$. So, the QC process surpasses the QCLC process. Thus, the QCM is useful to describe the PL mechanism of the system in this range of size of the particle as depicted in Fig. (4.1)[1].

When the most probable size of the NSP in the Si/SiO_2 system decreases both $\langle 1/\tau_{ar}\rangle$ and $\langle 1/\tau_{br}\rangle$ increases very fast. The $\langle 1/\tau_{ar}\rangle$ approximately increases as L_m^{-6} from equation (3.20), while $\langle 1/\tau_{br}\rangle$ increases approximately as L_m^{-4} from equation (3.21). As given in equation (3.21), σ_e^o (or σ_h^o), N_{LC} and η_{LC} are important parameters besides L_m for $\langle 1/\tau_{br}\rangle$. We have approximately,

$$\frac{\langle 1/\tau_{br}\rangle}{\langle 1/\tau_{ar}\rangle} \propto \sigma^o N_{LC} \eta_{LC} L_m^2. \tag{4.1}$$

Here $\sigma^o = \sigma_e^o$, when the LCs are neutral and $\sigma_e^o >> \sigma_h^o$, or the LCs are negatively charged before illumination.

From equation (4.1) it is observed that, for a nanoscale Si/SiO_2 system the larger the LC parameters σ^o, η_{LC}, N_{LC} and the larger the NSP most probable size,

[1] For the plot we have used the following values for: $m_l = 0.89m_o$, $m_t = 0.19m_o$, $m_h = 0.5m_o$ [26] , $\frac{|p_{cv}|^2}{2m_o} = 7eV$, $n = 1.33$ for p-Si of 75% porosity [14], $k_o = 0.85/a$ [25].

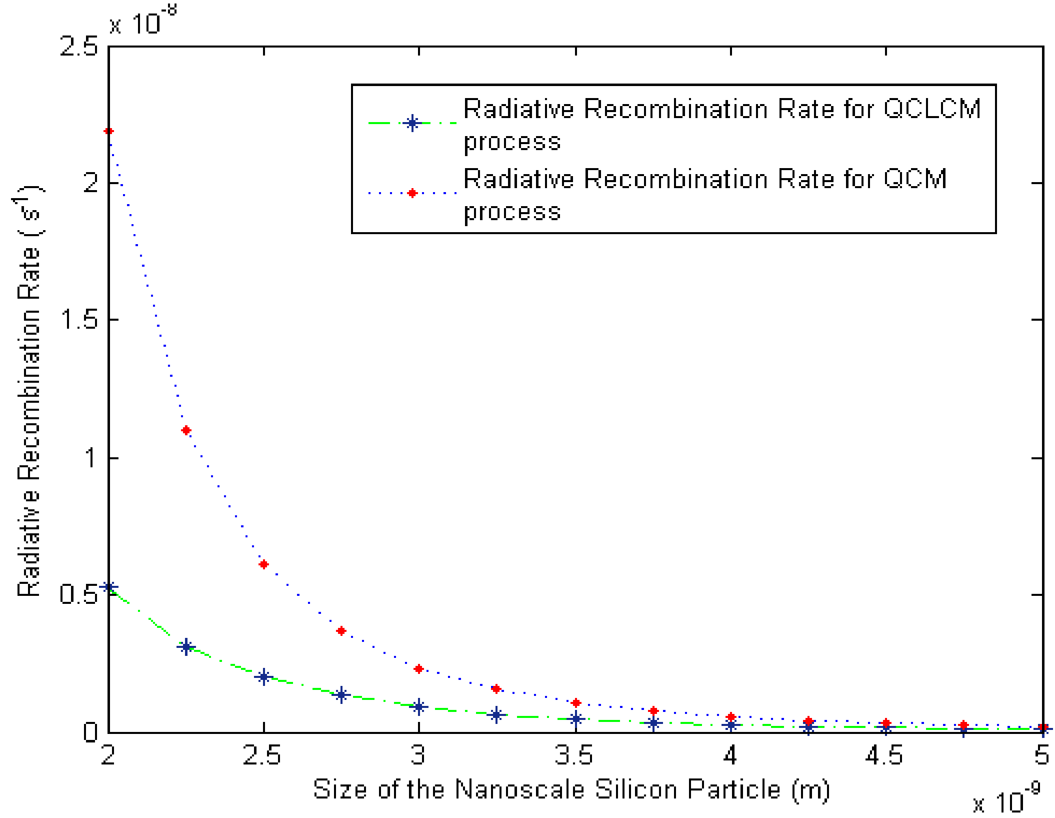

Figure 4.1: The dependance of the radiative recombination rates on the size of the NSP for the two types of processes, QCM and QCLCM processes (from Eqn.(3.2) and (3.13))

L_m, it is more favorable for the QCLC process to surpass the QC process and vise versa. For a specific type of LC in $\mathrm{SiO_2}$ the values of η_{LC} and σ^o are fixed with N_{LC} and L_m are the two active parameters which determine whether the QC or QCLC process plays a major role in PL. The larger the NSPs and the higher the density of LCs in SiO_2, the more favorable for the QCLC process than the QC process to occur, and vise versa.

4.3 Luminescence Center Density

For a nanoscale Si/SiO_2 system with definite N_{LC}, we can define a critical most probable size of the NSP, L_m^{crit}, just in a similar fashion as we define a critical LC density. When $L_m > L_m^{crit}$, we have $\langle 1/\tau_{br}\rangle > \langle 1/\tau_{ar}\rangle$, i.e., photoemission occurs mainly in the LCs in the SiO_2 and when $L_m < L_m^{crit}$, we have $\langle 1/\tau_{br}\rangle < \langle 1/\tau_{ar}\rangle$, i.e., photoemission occurs mainly inside the NSPs. Finally, for $\langle 1/\tau_{br}\rangle = \langle 1/\tau_{ar}\rangle$, $L_m = L_m^{crit}$. Though it is a difficult task to simplify the result, we can find the value of L_m^{crit} as a function of N_{LC}^{crit} from the above relation. We can also find the L_{LC}^{crit} from the plot in figure 4.2[2].

Figure 4.2 shows that for nanoscale Si/SiO_2 system with the ($N_{LC,}$ L_m) points just on the $N_{LC}^{crit} - L_m$ curve, we have $\langle 1/\tau_{br}\rangle = \langle 1/\tau_{ar}\rangle$, which indicates that the QC and QCLC processes have the same rate and the two models are equally important in describing the PL mechanism of the system. For the nanoscale Si/Si oxide systems with the ($N_{LC,}$ L_m) points at the left down side of the $N_{LC,}^{crit}$-L_m curve, we have $\langle 1/\tau_{ar}\rangle > \langle 1/\tau_{br}\rangle$, i.e., the QC process surpasses the QCLC process, and for a nanoscale Si/Si oxide with the ($N_{LC,}$ L_m) points at the right-up side of the N_{LC}^{crit}-L_m curve, we have $\langle 1/\tau_{ar}\rangle < \langle 1/\tau_{br}\rangle$, i.e., the QCLC process surpasses the QC process. If the (N_{LC}-L_m) points are near the N_{LC}^{crit}-L_m curve both the QC and QCLC processes should be considered at equal footing.

Experimentally different preparation techniques are used to obtain oxidized p-Si. Althogh preparation conditions and oxidation treatments for p-Si were very

[2]For the plot we have used the following values for: m$_l = 0.89m_o$, m$_t = 0.19m_o$, m$_h = 0.5m_o$,$U_{oe} = 4.6eV$ [26] , $\frac{|p_{cv}|^2}{2m_o} = 7eV$, σ_e^o=1×$10^{-19}m^2$, η_{LC} = 10% $n = 1.33$ for p-Si of 75% porosity [14], k$_o = 0.85/a$ [25],

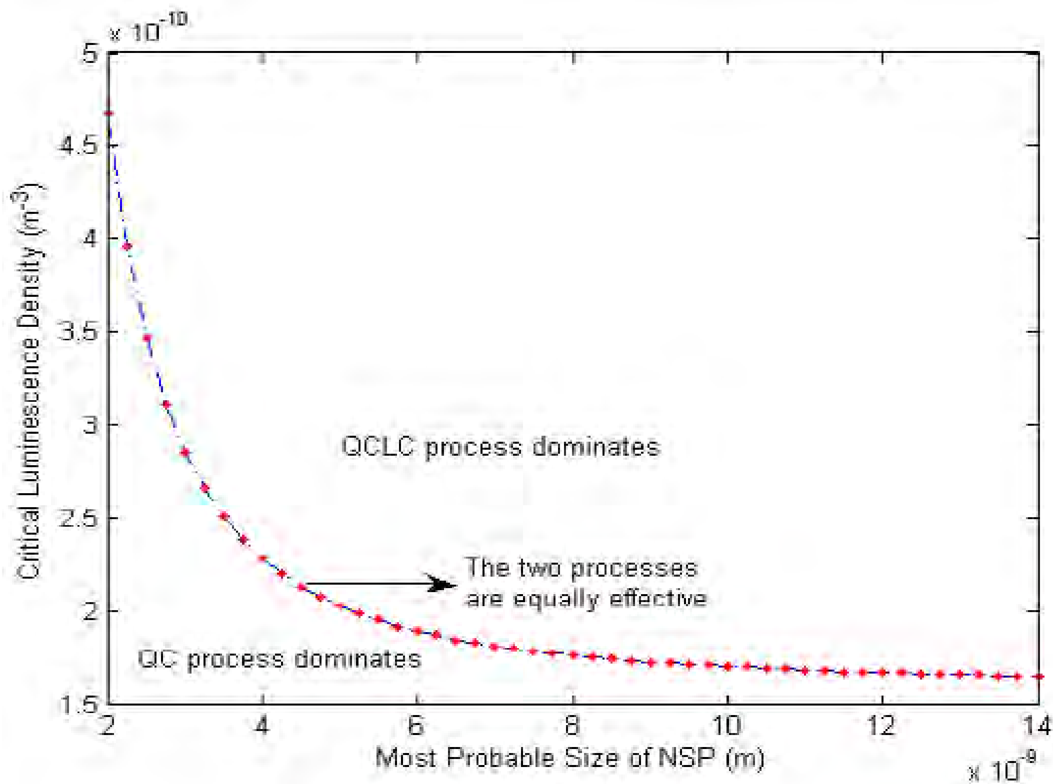

Figure 4.2: The critical luminescence density vs. the most probable size of the nanoscale silicon particle (from equation (3.22))

different, the experimental results in PL were consistent with each other [14]. Some of the experimental results can hardly be explained by process A, because NSPs will shrink after oxidation and the PL spectra from the p-Si should blue shift consistently. However, the result can be explained by process B and/or C. After oxidation, the supposed N_{LC} for LCs in the SiO_2 layer increased to exceed N_{LC}^{crit}, thus radiative process B surpassed A.

Koyama et al.[28] controlled the sizes of NSPs in p-Si kept in vacuum using post anodization illumination by white light and obtained a blue PL band. After exposing the p-Si to air for several seconds, a significant increase in the oxide layer

coverage of the p-Si surface was observed in XPS spectra, while the PL spectrum changed from blue to red [27]. Which means after oxidation the N_{LC} in equation (3.13) increases and so the radiative recombination rate for process B is larger than the radiative recombination rate of process A, hence, the QCLC process is more important.

The process A alone cannot explain the decay of NSPs due to oxidation, whereas the PL spectrum shift can be explained with this process. If we consider that, when the freshly prepared p-Si (being free from oxidation) was kept in a vacuum, Si-oxide on NSP surfaces is little, i.e., $N_{LC} \to 0$, thus $\langle 1/\tau_{br} \rangle \to 0$ from equation (3.13) and the radiative process A surpassed B. According to Canham [19], the band-band recombination of e-h pairs in NSPs with small sizes caused a blue PL band. Whenever the p-Si was exposed to air not only process A, but also processes B and C occurred. If the LCs with red photoemission satisfied the condition $N_{LC} > N_{LC}^{crit}$, the radiative process B with red photoemission surpasses process A with blue photoemission then the fact that the PL spectrum changed from blue to red is well understood.

It is clear from figure 4.1 that as L increases, the radiative recombination rates for both processes A and B, decreases rapidly and hence both processes are not important in this range of size of the NSP. For relatively larger size of the NSPs the process in which both the photoexcitation and photoemission occur in the LC is important process to describe the PL. In case of oxidised p-Si (N_{LC} is large), since the recombination rates in process A and process B depend on the photoexcited carriers in the NSP, we have, $P_{ar} \propto N_{NSP}\sigma^{o}_{NSP}\eta_{NSP}$ and $P_{br} \propto N_{NSP}\sigma^{o}_{NSP}\eta_{NSP}$. From equation

(3.23) the capture-cross section for the NSP become proportional to $L^2 f(\hbar\omega, E_{eh}(L))$, where $f(\hbar\omega, E_{eh}(L))$ is a function of $\hbar\omega$ (the photon energy of exciting light) and $E_{eh}(L)$ [13]. Provided typical samples have small L so that $\hbar\omega$ is no longer to be larger than $E_{eh}(L)$, such that the capture cross-section of the NSP will be zero; or NSP is very low. When a p-Si sample is oxidized at $1150^o C$, NSP disappear [28] and while LCs in the Si oxide still exist [13], in either case, P_{cr} surpasses both P_{br} and P_{ar}.

Chen et al. [27] discussed in detail about how the PL spectra in p-Si depend on the size of the NSP and surface states or the LCs in the SiO_2 layer. According to these observation, for Silicon particles kept in vacuum with various size distributions, the PL intensity increases as the particle size decreased but no peak shift was observed. However, for the particles with the average size of 5nm, it has the same PL but the absorption edge shifted. It was also noted that the PL intensity increased as the NSPs were aged. For particles larger than 9nm the peak remained unchanged (Fig. 4.3(left)) [28]. For particle of 5nm, however, the authors observed a blue shift of the peak to 7500 Å, (Fig. 4.3(right)).

It was also proposed that the QC effect is the possible mechanism of the PL of NSP when the particle size is smaller than 5nm [27]. This is the most important fact that we can extract from our work as indicated in figure 4.1. In their study, Chen et al. also observed that PL energies of the smaller particles (5nm), after aging showed peak shift in the wavelength rage from 6500 Å to 7700 Å. This is due to the reason that the size were further reduced to exhibit the QCE due to oxidation during

the aging. In contrary to this fact they mentioned that the PL of NSP was observed even when the particles were as large as 500nm.

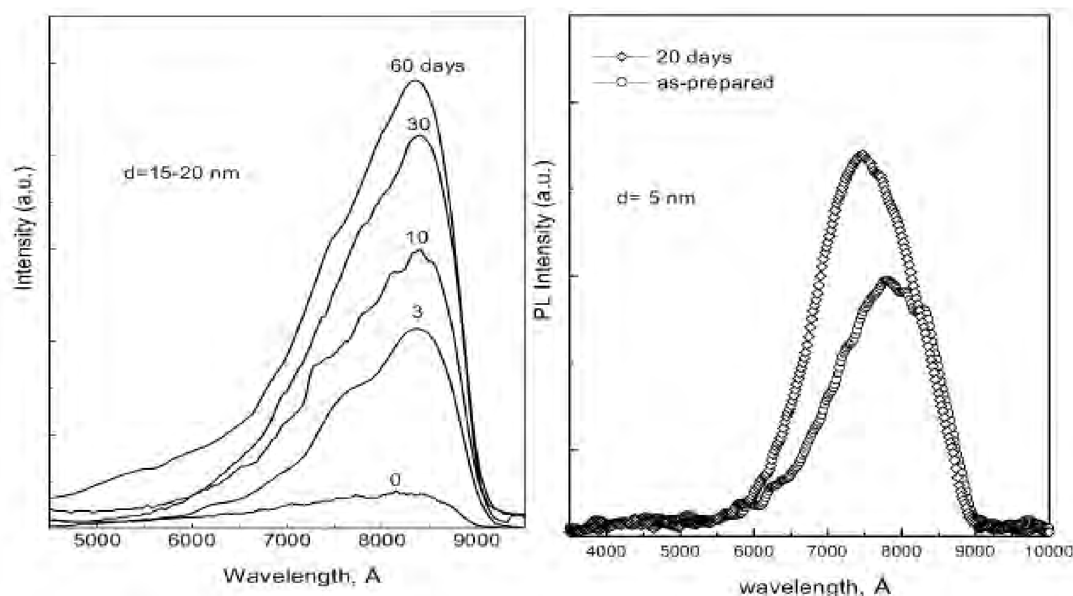

Figure 4.3: PL spectra of Si nanoparticles (L=15-20) (left). PL spectra of Si nanoparticles (average size 5nm). As prepared and after aging [27].

The Fourier Transform Infrared (FTIR) spectra and Energy Spectrum for Chemical Analysis (ESCA) study showed that the NSPs were covered with (oxide) oxygen and the amount of oxygen depend on the particle size. From the PL spectra there is a fixed peak position, and there is the increased intensity as particle size decreased, and as the aging time increased, i.e., the PL intensity increased as the amount of oxygen (oxide) increased. It implies that the surface layer played a key role in the visible light emission for larger nanoparticles.

The size dependent peak energies and strength of the dominant factors for the PL processes is shown in figure 4.4. The photoluminescence processes for larger

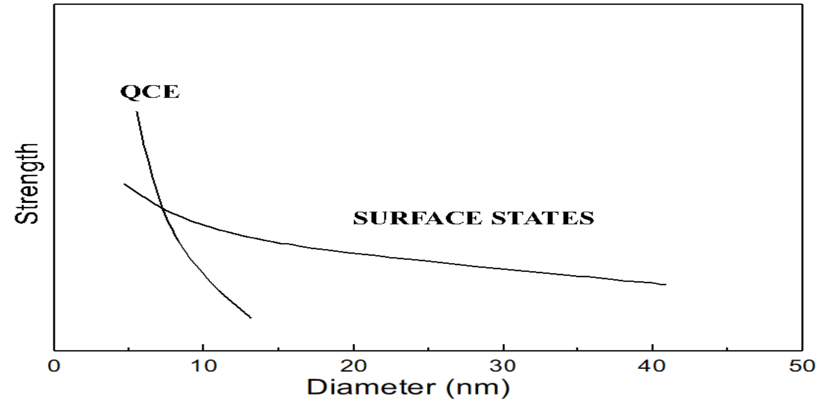

Figure 4.4: Schematic strength of the dominant factor in the PL [27].

sizes can be attributed to LCs or surface states in the SiO_2 layer. As the e-h pairs are generated by illumination light, light emission would be observed after the recombination of electrons and holes in the LCs.

The transition from the surface dominated to QCE dominated region, with particle size around 9nm, the PL could be operated by a combination of these two effects [27]. Thus, in order to describe the PL from Si/SiO_2 the System, multiple mechanism model is quite important. And hence our work is inconformity with what is done partly in [27]. Although there are many other issues like temperature dependence of luminescence peak and recombination rate that are not in the preview of our model. Our focus of attention was on the room temperature phenomena. There are some other proposal regarding PL in the recent years but there is no systematic way of understanding them. We therefore believe that our unified systematic approach clearly reflect some insight of the PL mechanism from nanoscale Si/SiO_2 systems [29, 30].

Chapter 5

Summary and Conclusion

In this thesis work we have verified the multiple mechanism model for the PL of oxidized porous Silicon. The two types of PL mechanism models, the QCM and QCLCM are used. Where by the PL from both pure nanoscale Silicon particle and nanosilicon particle embedded in SiO_2 matrix is clearly observed. We studied the PL of Si/SiO_2 system by calculating the radiative recombination rate for three competitive processes defined in relation to the PL mechanism models considered.

In the QCM process, process A, both the photoexcitation and photoemission occur in NSPs, in QCLCM process, process B, photoexcitation occurs in the NSPs, while the photoemission occurs in luminescence centers in a Si-oxide layer adjacent to the NSPs and in process C, both the photoexcitation and photoemission occur in the LCs. Out of all these, the process that plays the major role in the PL is determined by the oxidation degree of the p-Si sample. The main parameters of the LC in the Silicon oxide are the capture cross-sections, and the density of LC in the Si-oxide and the size of the NSPs.

For a p-Si sample free from oxidation, the QCM process dominates as reflected from our results, for most oxidized p-Si, the QCLCM process dominates. When NSPs in oxidized p-Si samples have very small density or large sizes, the process that both photoexcitation and photoemission occur in LCs in the Si-oxide layers is dominating.

For a nanoscale Si/SiO_2 system with a specific type of LC of definite density, a critical most probable size of the NSPs can be defined. If the most probable size of the NSPs is larger than the critical one the QCLCM process surpasses the QCM process, on the other hand if the most probable size of the NSPs is smaller than the critical one, the QCM process surpasses the QCLCM process. For a possible set of the parameters for nanoscale Si/SiO_2 system a $N_{LC}^{crit.}$ vs L_m curve can be plotted to examine the dependence. For a system with (N_{LC}, L_m) points just on the curve (red dots) the QC and QCLC model processes are equal in rate and equally important. For points to the left-down side of the curve (figure 4.2) the QCM process dominates and for a system with (N_{LC}, L_m) points to the right-up side of the curve the QCLCM process dominates. For a system with (N_{LC}, L_m) points close to the curve, both the QCM and QCLCM processes should be taken into account. This result is in confirmity with other observations.

In cnclusion, three competitive processes A, B and C occur in PL from oxidized porous Silicon an nanoscale Si/SiO_2 system are considered to explain experimentally observed PL spectra. For p-Si sample free from oxidation, radiative process A dominates, for most oxidized p-Si samples, radiative process B dominates, and for

oxidized porous Silicon samples with NSPs of very low density or large size radiative process C dominates. Thus, in order to explain the PL from oxidized p-Si and nanoscale Silicon particle embedded in Si/SiO_2 system, the above three processes should be considerd and more than one type of PL mechanism models are important [29, 30]. There are also some other issues related to PL worth to study.

Bibliography

[1] P. Bettotti, M. Cazzanelli, L. Dal Negro, B. Danese, Z. Gagurro, C. J. Oton, G.V. Prakash and L. Pavesi. J. Phys:Condens.Matt **14**, 8253-8281(2002).

[2] G. Asseffa. M.Sc thesis on Photoluminescence Mechanism in Silicon Nanostracture, Addis Ababa University, March (2007).

[3] Kengo Nishio, Junichiro Koga, Toshio Yamaguchi and Fumiko Yonezawa. Phys. Rev. B **67**, 195304(2003).

[4] Lorenzo Pavesi. Monograph on Photonics Applications of Nanosilicon, Universita di Trento-Italy, 2005.

[5] K.T. Tadesse. M.Sc project on Silicon Nanostructures. Addis Ababa University, 2006.

[6] http://www.osti.gov/bridge.

[7] http://www.library.unsw.edu.au/~thesis/adt-NUN/uploads/approved/adt-NUN20040105.171835/public/07chapter3.pdf .

[8] S. K. Ghoshal, Umesh Gupta and Karan Singh Gill. Indian J. Pure and App. Phys. **43**, 188-191(2005).

[9] D. Kovalev, H. Heckler, M. Ben-Chorin, G. Polisski, M. Schwartzkopff, and F. Koch1. Phys. Rev. Lett. **81**, 2803(1998).

[10] www.micronova.fi/units/epg/publications/publications2001/Reports25.pdf.

[11] S. Veprek. Thin Solid films **297,** 145-153(1997).

[12] N. Daldosso, M. Luppi, S. Ossieni, E. Degoli, R. Magri, G. Dalba, P. Fornasini, R. Grisenti, F. Rocca, L. Pavesi, S. Bonineilli, F. Priolo, C. Spinella, and F. Laeona. Phys.Rev. B **68**, 085327(2003).

[13] G.G. Qin and G. Qin. Phys. Status Solidi A **182**, 335(2000).

[14] G.G. Qin and Y.Q. Jia. Phys. Rev. B **68**, 085309(2003).

[15] J. Bai Xia and K.W. Cheah. Phys. Rev. B **56**, 14926(1997).

[16] M.V. Wolkin, J. Jorne, P.M. Fauchet, G. Allan and C. Delerue. Phys. Rev. Lett. **82**, 197(1999)

[17] D. Lockwood, M.W.C. Dharma-Wardana, Z.H. Lu, D.H. Grozea, P. Carrier and L.J. Lewis. Mat. Res. Soc. Symp. Proc. Vol. **737**(2003).

[18] D. Lockwood, Z.H. Lu, and J.M. Baribeau. Phys. Rev. Lett .**15**(1996).

[19] L.T. Canham. Appl. Phys. Lett. **57**, 1046(1990).

[20] S.M. Prokes. J. Mate. Res., Vol. **11**, No. 2, 1996.

[21] J.S. Biteen. PhD thesis on Plasmon-Enhaced Silicon Nanocrystals Luminescence for Optoelectronic Applications, California Institute of Tech., 2006.

[22] Y. Kanemitsu, H. Uto, Y. Masumoto, T. Matsumoto, T. Futagi, and H. Mimura. Phys. Rev. B **48,** 2827(1993).

[23] Md. N. Islam and Stayandra Kumar. J. Appl. Phys. **93**, 1753(2003).

[24] G.G. Qin and Y. Q. Jia. Solid State Commun. **86**, 559(1993).

[25] T. Oussie and A. G. Nassioipoulou, Erophys. Lett. **51(2)**, 168(2000).

[26] G.G. Qin and G.Qin. J. Appl. Phys. **82**, 2572(1997).

[27] H. S. Chen, J. J. Chiu and T. P. Perg. Mater. Phys. Mech. **4**,62-66 (2001).

[28] H. Koyama, H. Mizuno and N. Koshida, Appl. Phys. Lett. **69**, 3779(1996).

[29] T. Wondwosen and S.K. Ghoshal. Paper on Unified Model for Photoluminescence from Oxidized Porous Silicon and Nanosilicon Particle Embedded in Silicon-Oxide (in preparation) (2007).

[30] S.K. Ghoshal, K.P. Jain and S.R. Elliot. J. Met. Nano. Mat. **23**, 129(2005).